

2019

## Synthesis and Characterisation of Mesoporous Transition Metal Oxides Based on Soft-Templating Method

Hamzeh Q. Qutaish  
*University of Wollongong*

Follow this and additional works at: <https://ro.uow.edu.au/theses1>

### University of Wollongong

#### Copyright Warning

You may print or download ONE copy of this document for the purpose of your own research or study. The University does not authorise you to copy, communicate or otherwise make available electronically to any other person any copyright material contained on this site.

You are reminded of the following: This work is copyright. Apart from any use permitted under the Copyright Act 1968, no part of this work may be reproduced by any process, nor may any other exclusive right be exercised, without the permission of the author. Copyright owners are entitled to take legal action against persons who infringe their copyright. A reproduction of material that is protected by copyright may be a copyright infringement. A court may impose penalties and award damages in relation to offences and infringements relating to copyright material.

Higher penalties may apply, and higher damages may be awarded, for offences and infringements involving the conversion of material into digital or electronic form.

Unless otherwise indicated, the views expressed in this thesis are those of the author and do not necessarily represent the views of the University of Wollongong.

### Recommended Citation

Qutaish, Hamzeh Q., Synthesis and Characterisation of Mesoporous Transition Metal Oxides Based on Soft-Templating Method, Master of Philosophy thesis, Institute for Superconducting and Electronic Materials, University of Wollongong, 2019. <https://ro.uow.edu.au/theses1/495>

Research Online is the open access institutional repository for the University of Wollongong. For further information contact the UOW Library: [research-pubs@uow.edu.au](mailto:research-pubs@uow.edu.au)



# **Synthesis and Characterisation of Mesoporous Transition Metal Oxides Based on Soft-Templating Method**

Hamzeh Q. Qutaish

Supervisors:

Dr Md Shahriar Hossain

Prof Yusuke Yamauchi

Prof Jung Ho Kim

A/Prof Konstantin Konstantinov

This thesis is presented as part of the requirement for the conferral of the degree:  
Master of Philosophy

University of Wollongong  
Institute for Superconducting & Electronic Materials,  
Engineering and Information Sciences

March 2019

## Abstract

Mesoporous materials have attracted extensive interest in the past few decades because of their diverse applications in different fields, including chemical, environmental, energy, optics, electronics, medical and biotechnological applications. They display unique properties presumably because of their pores, which are sufficiently large to host large and/or multiple molecules, but not large enough for bulk properties to influence surface interaction. The mesoporous transition metal oxides group is among the mesoporous materials with several properties, including d-shell electrons confined to nanosized walls, redox active internal surfaces and connected pore networks. Among various transition metal oxides, nickel oxide (NiO), a wide bandgap (3.6–4.0 eV) p-type semiconductor, has gained significant attention owing to its exciting intrinsic properties, such as electrochromic, antiferromagnetic and high capacitive properties. In addition, NiO can be utilised in a wide range of applications, such as electrochromic display devices, smart windows, active optical fibres, gas sensors, solar thermal absorbers, catalysis, fuel cell electrodes, supercapacitors and energy storage devices.

The soft-templating method is used to synthesise mesoporous materials because it offers many benefits, including achieving cost-effectiveness, creating various porous networks with a wide range of pore sizes and providing access to well-defined morphologies and customisation for various applications. However, this method is extremely sensitive to hydrothermal conditions, such as concentration, temperature and pH. In addition, the synthesis process for some transition metal oxides has extra difficulties, including high tendency to build a stable structure with high lattice and possibility of structure collapsing on template removal.

In the present study, an asymmetric poly (styrene-block-acrylic acid-block-ethylene glycol) (PS-*b*-PAA-*b*-PEG) triblock copolymer is used as a soft template to synthesise the mesoporous NiO. In aqueous solutions, the block copolymer forms a micelle containing a PS core, a PAA shell and a PEG corona. The PS block serves as the core of the micelles because of its hydrophobicity, while the anionic PAA block interacts with the cationic Ni<sup>2+</sup> ions in the solution to form the shell and the PEG block forms the corona of the micelles.

The goal of the corona is to stabilise the micelles by avoiding secondary aggregation through steric repulsion between the PEG chains. The synthesised mesoporous NiO was characterised with different techniques, including x-ray diffraction, scanning electron microscopy, high-resolution transmission electron microscopy and the Brunauer–Emmett–Teller method. The NiO shows a large average pore size of 35 nm with a large specific surface area ( $97.0 \text{ m}^2 \text{ g}^{-1}$ ) and pore volume ( $0.411 \text{ cm}^3 \text{ g}^{-1}$ ). It is expected that the proposed soft-templating strategy could be generalised to other metal oxides/sulphides in the future for potential applications in gas sensors, environmental applications, catalysis, energy storage and conversion, optoelectronics and biomedical applications.

## **Acknowledgements**

It is my extreme pleasure to acknowledge the valuable assistance I received from all my friends and the employees at the Institute for Superconducting and Electronic Materials (ISEM), University of Wollongong, Australia, during my master's study.

I would like to thank my principal supervisor, Dr Md Shahriar Hossain, for his guidance, patience and support during the time of my master's study. I am appreciative of the massive encouragement that he has provided me. I would also like to thank my co-supervisor, Prof Yusuke Yamauchi, for his support and all the great, useful discussions.

Thanks to my co-supervisors, A/Prof Konstantin Konstantinov and Prof Jung Ho Kim, for their valuable advice, which helped me to accomplish my work.

Finally, I am much thankful to my family for their love and support.

## **Certification**

*I, Hamzeh Qutaish, declare that this thesis submitted in fulfilment of the requirements for the award of Master of Philosophy, from the Institute for Superconducting & Electronic Materials, Faculty of Engineering, University of Wollongong, is wholly my own work unless otherwise referenced or acknowledged. This document has not been submitted for qualifications at any other academic institution.*

Hamzeh Qutaish

25 March 2019

## List of Abbreviations

|                |   |
|----------------|---|
| AIBN           | Azobisisobutyronitrile  |
| BET            | Brunauer–Emmett–Teller  |
| BJH            | Barrett–Joyner–Halenda  |
| DLS            | Dynamic light scattering  |
| GPC            | Gel permeation chromatography   |
| HF             | Hydrogen fluoride   |
| ISEM           | Institute for Superconducting and Electronic Materials                              |
| LIB            | Lithium-ion battery   |
| MCM            | Mobil Composition of Matter   |
| NaOH           | Sodium hydroxide  |
| NiO            | Nickel oxide  |
| NMR            | Nuclear magnetic resonance  |
| PEG-CTA        | Poly (ethylene glycol) methyl ether (4-cyano-4-pentanoate dodecyl trithiocarbonate) |
| PS-b-PAA-b-PEG | Poly (styrene-block-acrylic acid-block-ethylene glycol)                             |
| PS-b-PEO       | Polystyrene-block-poly (ethylene oxide)   |
| SDA            | Structure-directing agent   |
| SEM            | Scanning electron microscopy  |
| TEM            | Transmission electron microscopy  |
| TGA            | Thermogravimetric analysis  |
| XRD            | X-ray diffraction   |

## List of Symbols

| Symbol         | Name  | Unit  |
|----------------|---|---|
| A              | surface area                                  | m <sup>2</sup> g <sup>-1</sup>                  |
| C <sub>p</sub> | polymer concentration                         | g L <sup>-1</sup>                               |
| D              | average crystallite size                      | nm  |
| DP             | degree of polymerisation                      | ppm   |
| FWHM           | full width at half maximum                    | radius  |
| L              | crystal size                                  | nm  |
| M <sub>n</sub> | number-average molecular mass                 | g mol <sup>-1</sup>                             |
| M <sub>v</sub> | viscosity molecular mass                      | g mol <sup>-1</sup>                             |
| M <sub>w</sub> | mass average molecular mass                   | g mol <sup>-1</sup>                             |
| M <sub>z</sub> | z-average molecular mass                      | g mol <sup>-1</sup>                             |
| N              | Avogadro's number = 6.022 × 10 <sup>-23</sup> | mol <sup>-1</sup>                               |
| n              | amount of the gas adsorbed                    | L   |
| P              | equilibrium pressure                          | P   |
| P <sub>0</sub> | saturation pressure                           | P   |
| R <sub>h</sub> | hydrodynamic radius                           | nm  |
| R <sub>p</sub> | pore radius                                   | nm  |
| T              | temperature                                   | K or °C   |
| t              | time  | h or s  |
| V              | volume  | M <sup>3</sup>                                  |
| 2θ             | peak position of XRD                          | °   |
| λ              | x-ray wavelength                              | Å   |
| μ              | electrophoretic mobility                      | cm <sup>2</sup> s <sup>-1</sup> V <sup>-1</sup> |
| ζ              | zeta potential                                | mV  |



# Table of Contents

|   |                              |
|---|------------------------------|
| <b>Abstract</b> .....   | <b>2</b>                     |
| <b>Acknowledgements</b> .....                                 | <b>4</b>                     |
| <b>Certification</b> .....                                    | <b>5</b>                     |
| <b>List of Abbreviations</b> .....                            | <b>6</b>                     |
| <b>List of Symbols</b> .....                                  | <b>7</b>                     |
| <b>Table of Contents</b> .....                                | <b>8</b>                     |
| <b>List of Tables</b> .....                                   | <b>10</b>                    |
| <b>List of Figures</b> .....                                  | <b>11</b>                    |
| <b>Dedication</b> .....                                       | Error! Bookmark not defined. |
| <b>Chapter 1: General Introduction</b> .....                  | <b>14</b>                    |
| 1.1 Introduction .....  | 14                           |
| 1.2 Research Background.....                                  | 14                           |
| 1.2.1 Pores and porosity .....                                | 14                           |
| 1.2.2 Classification of porous materials .....                | 15                           |
| 1.2.3 Use of mesoporous materials .....                       | 18                           |
| 1.3 Research Aims .....                                       | 19                           |
| 1.4 Thesis Structure.....                                     | 19                           |
| <b>Chapter 2: Literature Review</b> .....                     | <b>20</b>                    |
| 2.1 Synthesis of Mesoporous Materials .....                   | 20                           |
| 2.1.1 Top-down approach .....                                 | 20                           |
| 2.1.2 Bottom-up approach.....                                 | 21                           |
| 2.2 Mesoporous Metal Oxides .....                             | 30                           |
| 2.3 Applications of Mesoporous Metal Oxides.....              | 32                           |
| 2.3.1 Lithium-ion batteries.....                              | 32                           |
| 2.3.2 Supercapacitor.....                                     | 34                           |
| <b>Chapter 3: Techniques Used</b> .....                       | <b>36</b>                    |
| 3.1 Materials and Chemicals .....                             | 36                           |
| 3.2 Experimental Procedure .....                              | 37                           |
| 3.3 Preparation Approaches .....                              | 37                           |
| 3.3.1 Preparation of soft template .....                      | 37                           |
| 3.3.2 Synthesis mesoporous NiO by soft-templating method..... | 38                           |
| 3.4 Characterisation and Measurement Methods .....            | 39                           |
| 3.4.1 X-ray diffraction .....                                 | 40                           |
| 3.4.2 Scanning electron microscopy .....                      | 40                           |
| 3.4.3 Transmission electron microscopy.....                   | 41                           |
| 3.4.4 Thermogravimetric analysis.....                         | 42                           |
| 3.4.5 Nitrogen adsorption.....                                | 42                           |
| 3.4.6 Nuclear magnetic resonance spectroscopy .....           | 44                           |

|  |           |
|--|-----------|
| 3.4.7 Gel permeation chromatography.....   | 44        |
| 3.4.8 Measurement of zeta potential .....  | 45        |
| <b>Chapter 4: Soft-Templated Synthesis of Mesoporous Nickel Oxide Using Poly<br/>(styrene-<i>block</i>-acrylic acid-<i>block</i>-ethylene glycol) Block Copolymers .....</b> | <b>46</b> |
| 4.1 Introduction .....   | 47        |
| 4.2 Experimental Section .....   | 49        |
| 4.2.1 Chemicals.....   | 49        |
| 4.2.2 Preparation of PS402-b-PAA71-b-PEG46 triblock copolymer .....  | 50        |
| 4.2.3 Synthesis of mesoporous nickel oxide .....   | 51        |
| 4.3 Characterisation .....   | 51        |
| 4.4 Result and Discussion .....  | 53        |
| 4.5 Conclusion.....  | 63        |
| <b>Chapter 5: Conclusion .....</b>   | <b>64</b> |
| 5.1 Conclusion.....  | 64        |
| <b>References .....</b>  | <b>65</b> |
| <b>Appendix 1 .....</b>  | <b>79</b> |
| Peer Reviewed Articles .....   | 79        |
| Conference Proceedings.....  | 79        |

## List of Tables

|   |    |
|---|----|
| Table 3.1: Chemicals/Materials used to synthesise copolymer and mesoporous NiO .....  | 36 |
| Table 4.1: DP, $M_n$ and $M_w/M_n$ of PAA <sub>71</sub> - <i>b</i> -PEG <sub>46</sub> and PS <sub>402</sub> - <i>b</i> -PAA <sub>71</sub> - <i>b</i> -PEG <sub>46</sub> ..... | 50 |

## List of Figures

|   |    |
|---|----|
| Figure 1.1: Classification of porous materials by pore diameter [5].....  | 16 |
| Figure 1.2: Examples of classification of porous materials depending on their geometry ..   | 17 |
| Figure 2.1: Synthesis of mesoporous materials [58].....   | 23 |
| Figure 2.2: Block copolymer and the mechanism of producing mesoporous materials<br>[101] .....  | 26 |
| Figure 2.3: Effect of packing parameter on the geometry .....   | 27 |
| Figure 2.4: Mechanism of swelling agent (ethanol) to enlarge the pore size of carbon<br>[110] .....   | 28 |
| Figure 2.5: General procedure to synthesise porous materials using a hard-template<br>method [47] .....   | 29 |
| Figure 2.6: Diagram of lithium-ion battery.....   | 33 |
| Figure 2.7: Diagram of supercapacitor.....  | 34 |
| Figure 4.1: Synthesis route of PS <sub>402</sub> - <i>b</i> -PAA <sub>71</sub> - <i>b</i> -PEG <sub>46</sub> .....  | 50 |
| Figure 4.2: <sup>1</sup> H NMR spectra of (a) PAA <sub>71</sub> - <i>b</i> -PEG <sub>46</sub> in DMSO- <i>d</i> <sub>6</sub> at room temperature<br>and (b) PS <sub>402</sub> - <i>b</i> -PAA <sub>71</sub> - <i>b</i> -PEG <sub>46</sub> in DMF- <i>d</i> <sub>7</sub> at 120 °C ..... | 53 |
| Figure 4.3: GPC elution curves .....  | 54 |
| Figure 4.4: Hydrodynamic radius ( <i>R</i> <sub>h</sub> ) distribution of PS <sub>402</sub> - <i>b</i> -PAA <sub>71</sub> - <i>b</i> -PEG <sub>46</sub> in pure<br>water at pH 5.1 .....  | 55 |
| Figure 4.5: (a) TEM image of PS <sub>402</sub> - <i>b</i> -PAA <sub>71</sub> - <i>b</i> -PEG <sub>46</sub> in pure water at <i>C</i> <sub>p</sub> = 0.2 g L <sup>-1</sup> .<br>(b) Diameter distribution histogram of the polymeric micelles .....                                      | 55 |
| Figure 4.6: Schematic illustration showing the mechanism of the formation of<br>mesoporous NiO using the PS- <i>b</i> -PAA- <i>b</i> -PEG triblock copolymer template .....   | 56 |
| Figure 4.7: (a, c, e) SEM images and (b, d, f) the corresponding pore diameter<br>distributions of mesoporous NiO obtained using different amounts of nickel<br>salt: (a) 10 mg (0.0344 mmol), (b) 20 mg (0.0688 mmol) and (c) 30 mg<br>(0.1032 mmol).....                              | 57 |
| Figure 4.8: SEM images of the mesoporous NiO obtained at (a) 250 °C, (b) 350 °C and<br>(c) 450 °C .....   | 59 |

|   |    |
|---|----|
| Figure 4.9: (a) TEM and (b) high-resolution TEM images of mesoporous NiO obtained at an optimised calcination temperature of 350 °C (inset of (b): selected area electron diffraction).....   | 60 |
| Figure 4.10: TG curves of (a) PS-b-PAA-b-PEG triblock copolymer and (b) PS-b-PAA-b-PEG micelles (with Ni <sup>2+</sup> ). (c) Wide-angle XRD patterns for mesoporous NiO obtained at different calcination temperatures and (d) N <sub>2</sub> adsorption–desorption isotherms of mesoporous NiO obtained at the optimised calcination temperature of 350 °C..... | 61 |

## Dedication

*For my lovey family, who love and  
support me all the time*

# **Chapter 1: General Introduction**

## **1.1 Introduction**

As the Chinese proverb says, ‘With clay, we make a jar. But it is the empty space inside that we need’.

This saying underlines the impact of the early application of porous systems producing materials that have empty cavities. In the past, porous materials were acknowledged and used in several applications, including filtration and liquid adsorption. [1] For a long time, intensive efforts have been made to improve control of pore size, limit the pore diameter and optimise the shape organisation to enhance properties of the porous materials. [2-6] Therefore, nanoporous materials obtained their name from their nano-diameter pores, and their study is considered a vital branch of the science of nanostructured materials. These materials show a high specific surface area, large pore volume and rich surface chemistry. [7] The nanoporous materials present extensive potential and options for generation of various innovative, functional materials with enhanced properties, which have numerous applications in several fields, such as chemical, [4] environmental, [8] energy, [9] optics, [10] electronics, [11] medical [8] and biotechnological applications. [12]

Porous materials are materials that have a regular pattern of cavities, channels or interstices (pores). These materials present diverse geometries, structures and chemical compositions. [13-15]

## **1.2 Research Background**

### **1.2.1 Pores and porosity**

Generally, porous materials have a porosity between 2% and 95%. [16-21] The two fundamental types of pores are closed and open. [20] Closed pores have vacant cavities totally immersed in bulk materials, and these types of materials are used for thermal and sonic insulation. In contrast, open pores are associated with material surface and are used for separation, catalysis and sensing applications.

In open pores, surface roughness and pores should be distinguished. Therefore, pores are deep, rather than large, but in the case of surface roughness, the size is large, rather than deep and spreads out more than a pore. The differences between porous systems depend on porosity parameters, such as the ratio of pore volume to total material volume. [16, 21]

### 1.2.2 Classification of porous materials

There are three main classification systems of porous materials:

**1. Pore dimension:** An effective way to classify porous materials is measuring the diameter size of their pores, because numerous properties, such as adsorption and diffusion that are of interest in applications, are determined by pore size. According to the International Union of Pure and Applied Chemistry definition, porous materials can be classified into three main subgroups depending on their pore dimension ( $d$ ) [22-24]:

- a. Microporous materials ( $d < 2\text{nm}$ ); see Figure 1.1. Because the pore size is relatively small, these pores can host only tiny molecules, such as gas molecules, and are usually used in gas-storage materials and filtering membranes. These materials are characterised by high interaction properties and slow diffusion kinetics. [25]
- b. Mesoporous materials ( $2 < d < 50\text{ nm}$ ), as illustrated in Figure 1.1. The pore size for these materials is sufficiently large to host big molecules, such as biomolecules or aromatic systems. According to the pore sizes, these materials are usually used in systems such as adsorbing liquids and vapour systems or as catalyst systems. The diffusion kinetic depends on capillarity and the interactions between the wall and molecules after the pore filling. [26]
- c. Macroporous materials ( $d > 50\text{ nm}$ ), as presented in Figure 1.1. The pores in these materials are very large, allowing them to host larger molecules, such as biomolecules and polyaromatic systems. Owing to their pore size, these materials are usually used as storage and catalysis systems for quick diffusion of chemical species. [27]



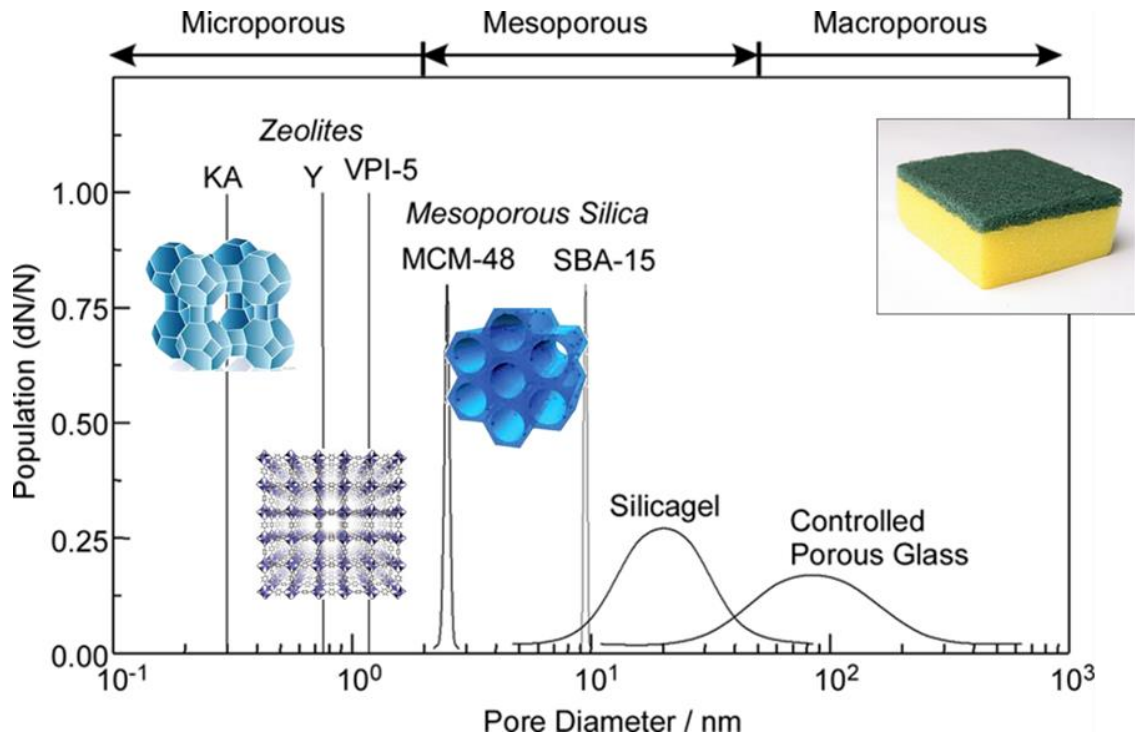


**Figure 1.1: Classification of porous materials by pore diameter [5]**

According to many studies of the size and shape of porous materials in real systems, pores cannot have a homogenous size and shape. In this case, microporous materials may possess additional mesopores due to random grain packing. Similarly, mesoporous materials could have additional macropores or micropores caused by the continuous network, and macropores could possess additional meso or micropores. These factors would be considered when materials are classified according to their homogeneity. A material that has just one type of pore could be more homogenous, even when the pores are disordered, than one having just a fraction of well-defined ordered pores. [28-30]

**2. Pore geometry:** Dimensionality depends on the shape and dimension of the pores. For example, pores with one or more non-nanoscale dimension are classified based on these dimensions as well as pore shape. Such classification is because of pore shape and dimensions, and it plays a vital role in the behaviour and application of the materials. [28-32]

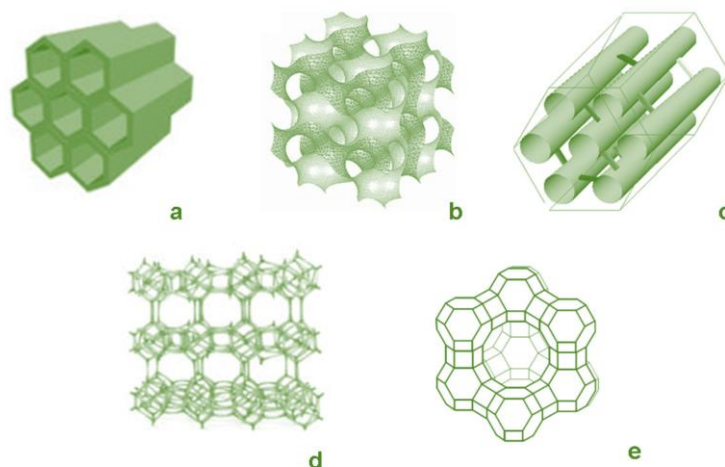


**Figure 1.2: Examples of classification of porous materials depending on their geometry** (a) parallel channel system (b) 3D interconnected pores (c) channels with secondary interconnections (d) 3D cage (e) single cage systems [33]As illustrated in Figure 1.2:

- 0D systems: All the pore dimensions are on the nanometric scale and are usually spherical. One famous example is zeolites. The various applications include to store single molecules and stabilisation of cavity interiors by three-dimensional interactions with walls. [34, 35]
- 1D systems: All pores are in the nanometric range, excluding one dimension that could be on the microscale. Usually, these systems are organised in a regular pattern, possibly hexagonal, and the channels may be curved, straight, isolated or connected. These materials are usually used as nanoreactors and for gas storage. One of the most famous examples is Mobil Composition of Matter-41 (MCM-41). [36]
- 2D systems: These systems have two non-nanometric dimensions; these materials are established by lamellae and usually separated by pillars. Main applications of these materials include intercalation with other materials, such as ions in electrical devices. One common example is MCM-50. [37, 38]
- 3D systems: These materials are created by complex structures of channels and/or cages that are interconnected to produce 3D structures. They are mostly utilised in storage systems or catalyst systems. [37, 39]

The number of nanometric dimensions influences material properties owing to the geometry of the system. [40] For instance, low-dimensional systems are used for their anisotropy. [41]

### **3. Chemical composition**

Classifying porous structures depending on the chemical structure of pore walls is quite difficult because of the large diversity of compositional materials. [42] However, chemical classification provides information about the chemical and mechanical properties of the sample. [2] Porous structures are typically categorised into organic, inorganic and hybrid porous systems. Organic porous materials are characterised by low mechanical and thermal resistance, [29, 43] whereas inorganic porous materials are chemically and thermally stable. Generally, organic porous materials are formed via aggregation of organic molecules, and these aggregates are stabilised by van der Waals interactions and/or hydrogen bonds. Inorganic porous materials are prepared *via* incorporation of inorganic substance, and since their structures are stabilised by strong covalent bonds, these can be utilised for their mechanical properties. [44, 45] Similar to the inorganic porous materials, hybrid materials are both chemically and thermally stable and have an advantage over the inorganic porous materials, in that a large variety of functional groups can be added. [46]

#### **1.2.3 Use of mesoporous materials**

Meso is a Greek prefix and means ‘in between’. On the nanometric scale, it implies *in between* the micro and macro range, and in this case, it means *in between* molecular and solid-state physics. Mesoporous structures are sufficiently large to host large and/or multiple molecules, but they are not large enough for bulk properties to influence surface interaction. Therefore, the mesostructures display unique properties, thus calling for investigation into the innovative properties and applications of these materials.

Mesoporous materials are particularly interesting because of the size of their pores, which can be accommodated by complex chemicals, molecular complexes and biomolecules. Further, mesoporous materials have a high surface area and a wide array of uniform morphologies and compositions. These properties play a vital role in catalysis and adsorbency and could be utilised in a wide range of sophisticated applications, such as

chemical, [43] environmental/energy, [44] optics, [45] electronics, [25] medical [46] and biotechnological applications. [47] For instance, zeolites are microporous materials used as adsorbents but are limited by their pore size. Thus, researchers are beginning to focus on mesoporous materials instead. [48-50]

### **1.3 Research Aims**

The aims of this thesis are summarised as follows:

1. to synthesise mesoporous materials with spatially distributed metal oxides using soft-templating method
2. to control the shape and size of the mesoporous structures by manipulating hydrothermal conditions
3. to characterise these materials by transmission electron microscopy (TEM), x-ray diffraction (XRD), scanning electron microscopy (SEM), the Brunauer–Emmett–Teller (BET) method, nuclear magnetic resonance (NMR) spectroscopy, gel permeation chromatography (GPC) and thermogravimetric analysis (TGA).

### **1.4 Thesis Structure**

This thesis is organised into four chapters. Chapter 2 presents a review of the literature on synthesis of mesoporous materials, which depends on two approaches. One is the so-called top-down approach, and the other is the bottom-up approach. In the bottom-up approach section, the soft-templating and hard-templating methods are described in detail because the study procedure mainly relies on these two methods. Chapter 2 also discusses mesoporous metal oxides and some energy storage applications, including lithium-ion batteries (LIBs) and supercapacitors. Chapter 3 demonstrates the experimental and characterisation methods, including chemical, synthetic procedures and physical characterisation techniques. Chapter 4 presents soft-templated synthesis of mesoporous nickel oxide using poly (styrene-block-acrylic acid-block-ethylene glycol) block copolymers. The general conclusions of the work and future research directions are presented in Chapter 5

## **Chapter 2: Literature Review**

### **2.1 Synthesis of Mesoporous Materials**

The synthesis of mesoporous structures requires controlling the structure at the nanoscale range. [51] To produce materials with innovative functions and structures, nanoarchitectonics, rather than nanofabrication, should be used. Nanoarchitectonics is proposed as a new, cutting-edge concept for the assembly of nanoscaled structural materials with a well-defined configuration. [49] Therefore, in-depth understanding of the interactions between materials, used to synthesise mesostructures, and their arbitrary arrangement, including manipulation of atoms and molecules, functional materials and sophisticated internal architectures, is required as well. [12, 35, 36]

All synthesis of nanostructured materials follows one of two pathways: the top-down approach or the bottom-up approach. In the case of mesostructured materials, creating mesopores in bulk materials requires a top-down approach, whereas creating mesopores by synthesising materials is performed utilising the bottom-up approach. [49, 52, 53]

#### **2.1.1 Top-down approach**

In this approach, physical and chemical etching, termed nanolithography, are utilised to produce mesopores from poreless materials. [54-57] This physical etching method depends on creating pores in a process termed ablation with focused laser pulse and electron or ion beams. The pore deepness can be precisely calculated from the ablation rate. However, when the ablation device is positioned near the material, the performance is limited owing to mechanical sensibility. In addition, using the chemical etching method, the mesopores can be obtained by corrosion of bulk materials with chemicals, such as acid and base. In this method, the poreless materials should be covered by a mask that is resistive to chemical etching for avoiding ablation of the entire surface. However, the application of this method is limited, presumably because of the difficulty in controlling the rate of ablation even after accounting for the concentration of the chemicals, and temperature and nature of the materials. [60]

The top-down approach is limited since pores cannot be interconnected for these are created at the material surface. Further, this method is expensive owing to the high price of technology and the cost of special masks, and it is not effective on some polymers and metal oxides. [61]

### **2.1.2 Bottom-up approach**

Chemical methods act as the main base for bottom-up approaches, where precursors react or organise to create pore structures. [58, 59] Pores can be obtained by two main methods. First, the precursor materials self-assemble to create porous supramolecular structures. [60, 61] Second, precursors condense around the template; then, these are removed by calcination, ozone treatment or other means, to form pores. [62, 63]

In the first case, intramolecular interactions, such as dipole–dipole interactions or van der Waals forces, stabilise the materials while the pores are formed because the precursors are arranged into conformations depending on temperature, nature of the materials and pH. [64, 65] The goal is to maximise the interaction between the molecules themselves, which results in well-defined pores and porosity. There are simple methods to obtain supramolecular aggregates, including slow cooling of an oversaturated solution, where the porous structures can be obtained by evaporation and filtration of the solvent. [66, 67] This method is reproducible because of the weak interaction between the molecules, allowing the molecules to redissolve and reproduce the suitable structures easily. However, this method is limited because it depends on the weak interaction between molecules, and hence, it is difficult to obtain beneficial materials required for applications. In addition, it is difficult to obtain real hybrids and functionalisation. [27, 40]

In the second case, precursors condense around templates or structure-directing agents (SDAs), which could be supramolecular aggregations, organic molecules or solid structures, and form pore structures after removing the SDAs (if necessary). [68, 69] The templating process offers many advantages, particularly that of nonspecific interactions, such that the same templates can be used for a large number of syntheses with different materials. However, this templating method is sensitive to concentration, temperature and pH. [70-72] Another advantage of this method is its cost-effectiveness and potential for

customisation for various applications. [73, 74] Further, templating, especially with soft templates, can synthesise materials with several porous networks with a wide range of pore sizes as well as well-defined morphologies on controllable length scales and geometries. This literature review examines the synthesis of mesoporous materials using amphiphilic molecules as soft templates as well as the hard-templating method. [75]

### **1. Soft template**

In soft templates, organic molecules are used as a ‘template’ and surrounded by a framework. [76-78] Removal of these organic molecules reveals a cavity that retains the same morphology and structure of the organic molecules.

Mesoporous metal oxides are obtained from organic–inorganic assembly, including surfactants and block copolymers as amphiphilic materials. [43] The hybridisation between inorganic structures and organic templates possess many benefits, including fine structuring of inorganic materials and mechanical strengthening of organic functional structures. [79]

Two main strategies are used to transcribe soft templates into inorganic materials. The first is hybridisation between rigid materials and soft-templating assemblies, and the second is structural transcription of the soft template into a rigid material. [5, 80]

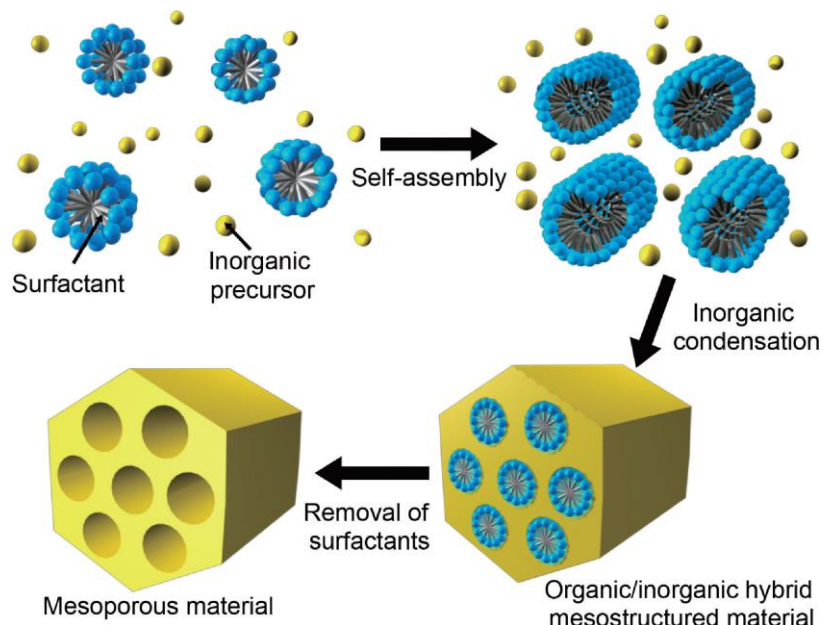


**Figure 2.1: Synthesis of mesoporous materials [58]**

Use of amphiphilic molecules is considered a common method to synthesise ordered mesoporous materials. [5, 81] Amphiphilic molecules contain a hydrophilic head and hydrophobic tail. Normally, the head moieties can be classified depending on their charge into cationic, anionic, cationic–cationic, cationic–anionic and non-ionic species. Various morphologies can be obtained from amphiphilic molecules because they can spontaneously self-assemble into aggregates, which are disordered on the atomic or molecular scale but display a periodical mesoscopic structure in varying shapes, including spherical and rod shapes. The aggregates can be used as SDAs for porous materials, [5, 82] as illustrated in Figure 2.1.

Kuroda et al. were the first to report successful synthesis of mesostructured materials (KSW-1) in 1990. In this case, they utilised the intercalated complex of a layered polysilicate kanemite with alkyltrimethylammonium cationic surfactants (Cn-TMA) to form mesoporous silica successfully. [83]

In 1992, a Mobil group achieved an important step in synthesising mesoporous materials using the templating method. Highly concentrated alkyltrimethylammonium bromide (Cn-TAB) or chloride (Cn-TAC) as removable templates for forming the liquid-crystal phase,



which were used with sodium silicate as silica source under basic conditions, which the inorganic materials introduced on surface of micelles to form mesostructured composites. [84, 85] For example, these materials have two-dimensional hexagonal (MCM-41), bicontinuous cubic (MCM-48) and lamellar (MCM-50) mesostructures. Many publications have followed this trend, and several are significant to the development of this field. [86, 87]

#### **a. Synthesis mechanism of mesoporous materials by surfactant as a soft template**

The successful preparation of highly ordered mesoporous siliceous materials led to adaptation of these methods for synthesis of other materials, such as metals and metal oxides. [4, 88] Importantly, the strong interaction between the template and inorganic materials can yield high ordered mesostructured materials. Electrostatic, van der Waals, hydrogen and coordination bonding interactions are involved. [89] For example, in using silica as the inorganic material, considering its negative charge, a cationic surfactant is preferred as a template. Therefore, in choosing a template, many factors are considered, including a selection of suitably charged inorganic materials.

Stucky et al. suggested four general synthetic routes:  $S^+I^-$ ,  $S^-I^+$ ,  $S^+X^-I^+$  and  $S^-X^+I^-$ , where (S) is a surfactant, I is an inorganic precursor and X is a mediator or counter ion. [90-92]

Adjusting the surfactant ionisation state, which is required for the inorganic part, is an important factor to synthesise efficient mesoporous materials. For example, under alkaline pH, silicate anions ( $I^-$ ) attract surfactant cations ( $S^+$ ) through Coulomb forces to form  $S^+I^-$ . The assembly of polyacid anions and surfactant cations to 'salt'-like mesostructures is also an  $S^+I^-$  interaction. An example of  $S^-I^+$  interactions is that between anionic surfactants, such as dodecyl benzenesulphonate salt, and the cationic Keggin ion  $Al^{137+}$ . [93]

It was reported that the organic–inorganic assembly of surfactants and inorganic precursors that share the same charge can occur in the presence of mediator or counter ions. For example, when synthesising mesoporous silicates by the  $S^+X^-I^+$  interaction,  $S^+$  and  $I^+$  have the same charge, whereas X is a negatively charged ion, such as halogens (chloride, bromide and iodine), a sulphate or a nitrate. [94]

The first mesoporous silica was prepared under acidic conditions by utilising the initial  $S^+X^-I^+$  interaction. This concept has been exploited for the synthesis of mesoporous zirconium oxophosphate, using alkyl ammonium ions as a surfactant and zirconium sulphate as a mediator. [95]

In the neutral surfactant ( $S^0I^0$ ) case, Pinnavaia and coworkers showed that polyethylene oxide (PEO) surfactants under neutral conditions can also be used as templates to develop the so-called MSU-X, which is a type of disordered mesoporous materials. [96] Covalent bonds can also mediate organic–inorganic interactions. [28, 97-100]

#### **b. Synthesis mechanism of mesoporous materials by copolymer as a soft template**

Laboratory block copolymers have been developed by Yamauchi and coworkers, including poly (styrene-*b*-acrylic acid-*b*-ethylene oxide) (PS-*b*-PVP-*b*-PEO). [101] In such copolymers, the inorganic precursors are strongly condensed on the hydrophilic part (PVP). The hydrophobic part (PS) plays a crucial role to adjust the phase diagram of the copolymer, and in the Yamauchi case, these blocks are frozen to form a spherical micelle. The adjustment of the fraction of the hydrophobic and hydrophilic blocks can result in different phase diagram structures. The (PEO) blocks work as stabilisers for the micelles in the solution by keeping them dispersed and maintaining the mesostructure during evaporation of the solvent [101, 102] as illustrated in Figure 2.2.

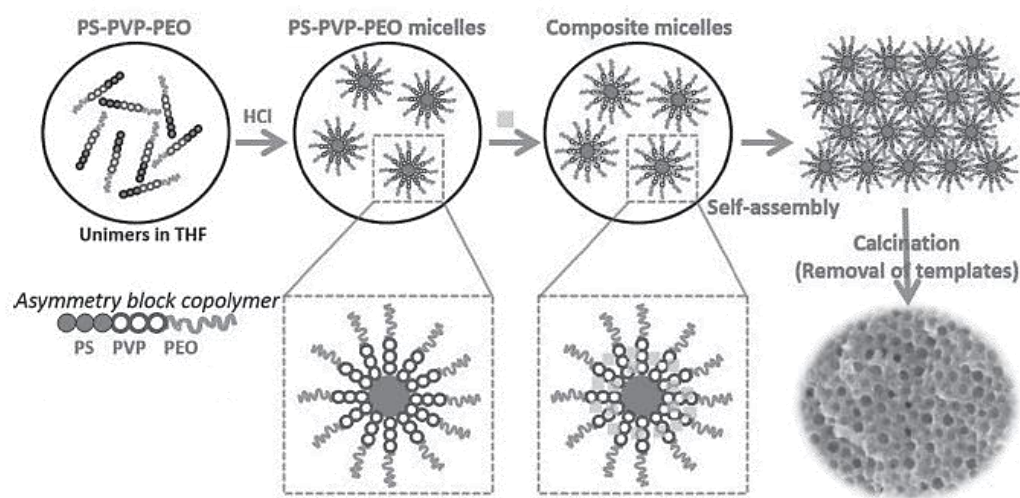


**Figure 2.2: Block copolymer and the mechanism of producing mesoporous materials [101]**

Stucky and coworkers used the diblock copolymer (ethylene oxide-butyleneoxide) (EO-BO) or triblock copolymer (ethylene oxide-propylene oxide-ethylene oxide) (EO-PO-EO) to successfully afford SBA-15. [103] In this process, it was important to use alcohol as a solvent because it is difficult to control hydrolytic conditions for different precursors and the condensation rate. In this work, the metal ions are condensed on the PO block, which together form a mesophase resulting from the difference in polarities of the EO and PO blocks, resulting in mesostructured materials. [73, 97, 101, 104, 105]

### c. Controlling pore geometry and size using a soft template

In terms of controlling the geometry of pores using surfactants, the lowest concentration of surfactants is termed critical micelle concentration, where the micelles are spontaneously created. [106] In the case of ionic surfactants, the critical micelle concentration is influenced by the ionic strength of the solution, while in case of non-ionic surfactants it is mainly temperature dependent. At higher amphiphilic concentrations, the randomly disordered micelles spontaneously assemble into liquid-crystal phases of differing structures, such as hexagonal, cubic or cylinder. The critical packing parameter (C<sub>pp</sub>) is utilised to assume the structure and conditions for possible phase transitions according to the following equation, as illustrated in Figure 2.3.

$$C_{pp} = \frac{V}{A_0 l_c} \quad (2.1)$$

Here,  $V$  is the effective volume of the hydrophobic chain,  $A_0$  is the optimal surface area and  $l_c$  is the critical chain length. The variables in the equation are dependent on temperature, surfactant concentration, ionic strength or pH. Usually, hexagonal and cubic phases occur when  $C_{pp} < 1/2$ , cylinder phases when  $1/3 < C_{pp} < 1/2$  and hexagonal and cubic inverse-type phases when  $C_{pp} > 1$ .

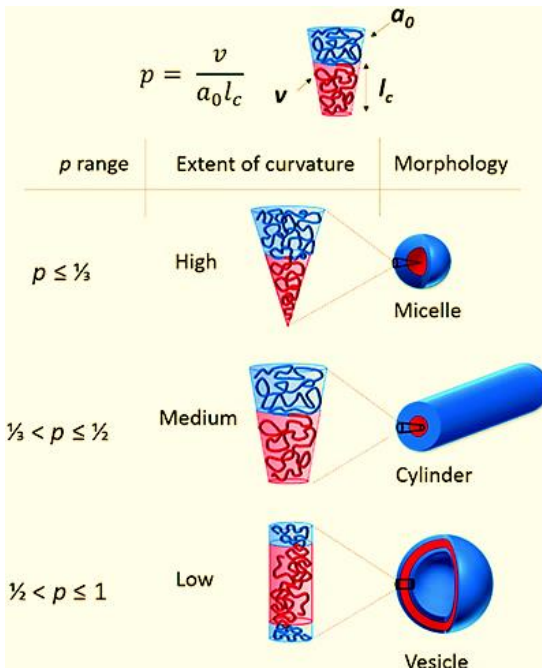


**Figure 2.3: Effect of packing parameter on the geometry**

In terms of control of the geometry of the pores using copolymers, the synthesis of mesoporous materials should be adapted according to the nature of materials, fraction of concentration between the copolymers and precursors, pH and temperature. [5]

The need for large size pores with increasing surface area for many applications, such as drug delivery, led to investigations on the effect of increasing the molecular weight of SDAs. [107, 108] In this case, the block copolymer poly (ethylene oxide)-b-poly (propylene oxide)-b-poly (ethylene oxide) (PEO-PPO-PEO) is commercially available as Pluronic P123 (EO20PO70EO20) and Pluronic F127 (EO106PO70EO106). The size of mesopores obtained is limited to a maximum of 8 nm owing to the relatively small

difference of hydrophobicity between the PEO and the PPO blocks and their molecular weights. [109]

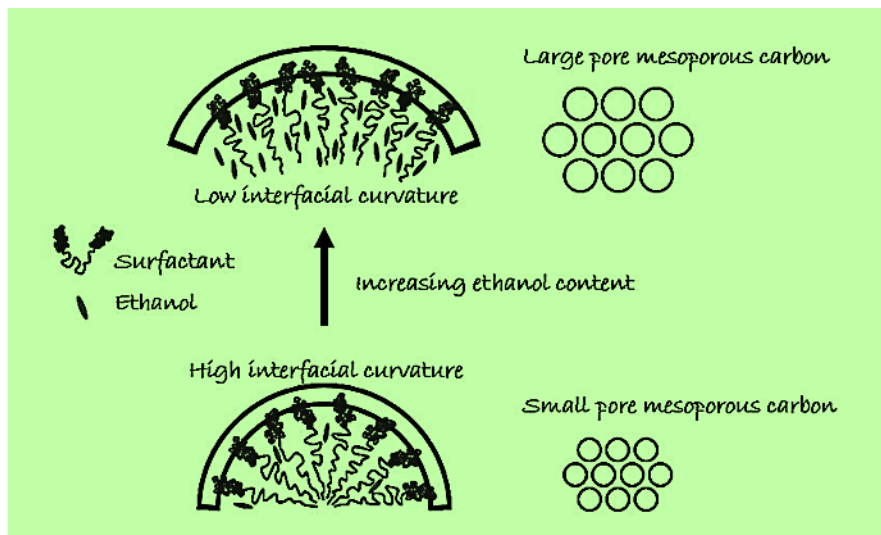


**Figure 2.4: Mechanism of swelling agent (ethanol) to enlarge the pore size of carbon [110]** After that, a hydrophilic swelling agent, such as 1, 3, 5-trimethylbenzene, is added to increase the mesopore size by penetrating the hydrophobic moieties of SDAs, as illustrated in Figure 2.4.

Then, the change of hydrophobicity with high molecular weight plays a vital factor to increase the size of mesopores, such as polystyrene-b-poly (ethylene oxide) (PS-b-PEO). [111]

In another study, various polymers, including poly (styrene-b-2-vinylpyridine-b-ethylene oxide) (PS-b-PVP-b-PEO), were used, emphasising that the average pore size and wall thickness can be easily tuned to several nanometres by varying the hydrophobic part lengths and the metal precursor concentration, respectively. The fine control over the crystallinity, pore size and wall thickness can provide remarkable insights on the performance of such mesoporous materials in diverse applications. [5, 112]

## 2. Hard template

The hard-template method, also known as the nanocasting, exotemplating or repeated templating method, is essential for the preparation of mesoporous materials because it

provides a stable mesoporous structure and allows for the synthesis of novel mesostructured materials. [113] Many hard templates are used, including anodic aluminium oxide (AAO), [114] polymeric microspheres [115] and silica. [116]

Generally, useful mesostructured materials are obtained through three steps, as shown in Figure 2.5. The first is synthesis of a sacrificial template with the desired porous structure, such as mesoporous silica MCM-48 for preparation of 3D of mesoporous carbon (CMK-1). [117, 118] The second is the formation of a hybrid composition of the original template and a target product through in situ deposition target precursors into the ordered pores, co-deposition and assembly of core-shell nanostructures. The final step is removing the original template to leave behind its metal replica. For example, sodium hydroxide (NaOH) and hydrogen fluoride (HF) solution or calcination can remove the original template. [9, 47]

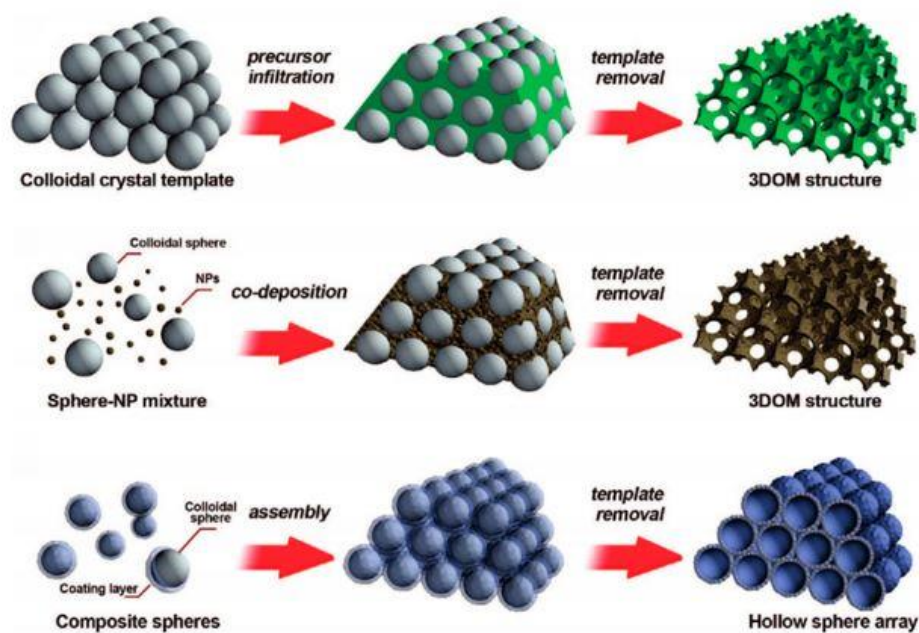


**Figure 2.5: General procedure to synthesise porous materials using a hard-template method [47]**

Polymeric beads are also utilised as hard templates because of their rigid structure. [119] In the Xu et al. report, polymethyl methacrylate was successfully used as a hierarchically ordered colloidal template to synthesise three-dimensionally-ordered macroporous

$\text{LaCo}_x\text{Fe}_{1-x}\text{O}_3$ . [120] Generally, template removal is executed by dissolution by solvents, calcination or pyrolysis. Silica is often served as a hard template to fabricate porous metal oxides because of its adaptable morphology and adjustable size. [121]

### **3. Comparison between the soft and hard template**

The soft template method possesses many advantages, including cost-effectiveness, ease of preparation under mild conditions and accessibility of a variety of mesoporous structures. Conversely, it has some disadvantages, including a fundamental dependence on complicated sol-gel processes and difficulties related to controlling polymerisation and hydrolysis of transition metal ions within the preparation process. The products of the soft template method may possess amorphous or semicrystalline walls with poor thermal and mechanical stability, and the preparation is commonly sensitive to relative humidity, especially when using commercial PEO-based copolymers. [91] Using silica to coat the internal and external surfaces of the amorphous materials is a method suggested to support the structure for obtaining a high crystalline structure. Then, calcination at high temperature is performed to crystallise the mesoporous materials, while the silica layers are removed under basic conditions. [92-95]

The hard-template method provides more accessibility for synthesising the desired mesoporous structures. Good quality mesoporous metal oxides with highly crystalline walls could be obtained using this method. This may be because mesoporous silica can offer more stability at high temperatures, allowing several metal oxides to crystallise. However, the method has certain disadvantages. First, the targeting mesoporous metal oxides should be resistant to the NaOH or HF solutions utilised to eliminate the silica template. [125-127] Second, because of the complex interactions between the silica and filtrated metal ion precursor, it is difficult to fill the mesoporous silica template completely. Other disadvantages include the multi-step synthesis and long reaction times. [124]

## **2.2 Mesoporous Metal Oxides**

Mesoporous transition metal oxides have gained significant attention over the past two decades owing to their versatile applications, including energy conversion, catalysis,

storage and magnetic applications. [25] Their versatile usage in a wide of range applications is mainly because of their unique properties, such as d-shell electrons confined to nanosized walls, connected pore networks and redox active internal surfaces. [9, 108]

Many important candidates are available in this group of materials; a brief description of the most common metal oxides follows:

- Nickel oxide (NiO) is one of the most important candidates among the transition metal oxides because its properties include it being transparent, conductive, electrochromic, antiferromagnetic and highly capacitive. Therefore, it has versatile applications, including electrochromic display devices, supercapacitors, gas sensors, solar thermal absorbers, photoelectrolysis, batteries and fuel cell electrodes. The preparation of ordered mesoporous NiO using the soft-templating method was first reported with pore sizes ranging from 4 to 7 nm by Banerjee et al. [128] The preparation of mesoporous NiO with crystalline walls and a well-defined pore structure was reported by utilising KIT-6 as a hard template. [129]
- Cobalt oxide ( $\text{Co}_3\text{O}_4$ ) is considered a material with technical applications, such as LIBs, [130] gas sensors [131] and electrochromic devices. [132] The small crystal size and the large surface area in the nanostructured  $\text{Co}_3\text{O}_4$  can enhance their catalytic reactivity and electrochemical activity. Various types of mesoporous silica have been used as hard templates to fabricate ordered mesoporous  $\text{Co}_3\text{O}_4$ , including SBA-15, [133] KIT-6 [134] and FDU-5. [135] The soft-templating method of synthesising  $\text{Co}_3\text{O}_4$  was introduced by Dahal et al., wherein ordered hexagonal mesoporous  $\text{Co}_3\text{O}_4$  is prepared utilising Pluronic P123 as a soft template.  $\text{Co}_3\text{O}_4$  has a large surface area with a tunable hexagonal structure. [110, 111]
- Iron oxides that have been synthesised by both hard and soft processes possess many applications in drug delivery systems, catalysis and magnetic storage as well as in LIBs. [112-114] By applying the soft-templating method, Smarsly et al. [136] introduced the preparation of crack-free mesoporous  $\alpha\text{-Fe}_2\text{O}_3$  and  $\alpha\text{-FeOOH}$  thin films, using the diblock copolymer poly (isobutylene)-block poly (ethylene oxide) (PIB-b-PEO) as a template. Mesoporous silica SBA-15 and KIT-6 have been utilised as hard templates to synthesise tunable mesoporous iron oxides. Further, a



series of ordered mesoporous iron oxides with different phases, including  $\alpha$ -Fe<sub>2</sub>O<sub>3</sub> [137] and  $\gamma$ -Fe<sub>2</sub>O<sub>3</sub>, [138] were synthesised.

- Ruthenium oxide (RuO<sub>2</sub>) is considered one of the most promising electrode materials for energy storage systems. The synthesis of mesoporous RuO<sub>2</sub> thin films with high capacitance value 1000 F g<sup>-1</sup> using the soft-templating method was reported by Sassoie, C. et al., using polymeric micelles made of amphiphilic PS-b-PEO block copolymers. [122] By controlling the surface hydrophobicity and application of the hard-templating method, synthesis of an ordered mesoporous RuO<sub>2</sub> was accomplished. [123]

## **2.3 Applications of Mesoporous Metal Oxides**

Mesoporous metal oxides are promising anode and electrode materials for LIB and supercapacitors, respectively. The importance of these materials in developing electrode materials is their energy storage properties.

### **2.3.1 Lithium-ion batteries**

LIBs are an efficient energy storage system used in portable electronic devices. The materials currently used in such systems are carbon-based, in particular graphite. [124] Graphite materials are used as anodes in such batteries because of their low cost, excellent electrical conductivity and high cycling stability. However, using carbon-based materials has many disadvantages, such as low capacity and inferior rate capability resulting from its poor lithium-ion diffusion coefficient.

Despite the widespread usage and fast growth of LIBs, enhancing their performance is critical, including increasing life cycle, reducing cost and improving safety. Many studies have been performed to find suitable and efficient materials. One of the most important candidate materials is mesoporous metal oxides. [125]

Mesoporous metal oxides have many properties, including large surface area, good availability, high theoretical capacitance, thin (nanometre scale) walls that ensure short diffusion distances for Li<sup>+</sup> on intercalation leading to fast electrode reactions, ability of the

electrolyte to flood pores leading to a high electrolyte–electrode contact area resulting in fast electrode reactions, and high packing density. See Figure 2.6.

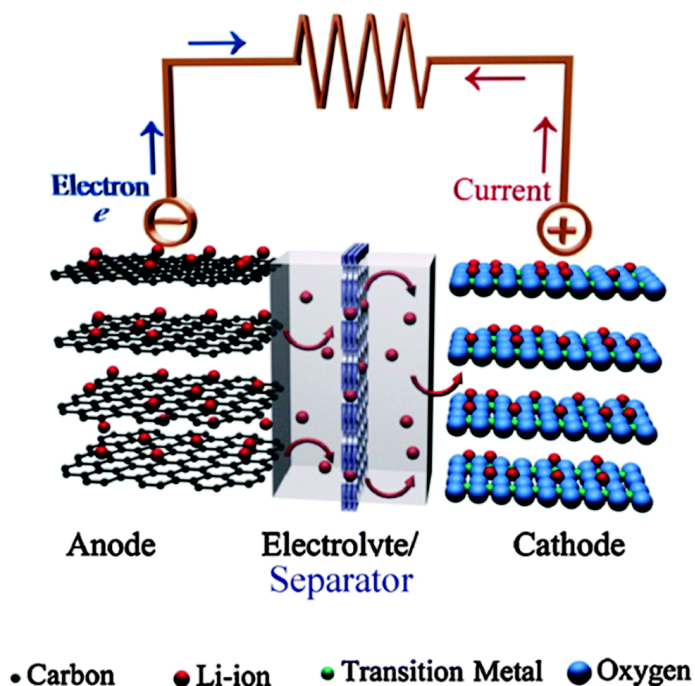


**Figure 2.6: Diagram of lithium-ion battery**

Efforts have been made to enhance anode materials using metal oxides or hybrid metal oxides with carbon materials. Wang et al. synthesised an anode from ordered mesoporous SnO<sub>2</sub>. The specific capacity was higher than that obtained from SnO<sub>2</sub> nanoparticles. Liu et al. utilised an ordered mesoporous NiO as an anode, and the results showed a higher specific capacity of 680 mA h g<sup>-1</sup> (at 0.1C) compared with that of commercial bulk NiO, which is only 188 mA h g<sup>-1</sup>. Bruce and coworkers showed that the Co<sub>3</sub>O<sub>4</sub> anode has considerable advantages over other forms of Co<sub>3</sub>O<sub>4</sub> (nanowire, nanoparticle and microparticle) regarding both specific capacity and cyclability. Chen et al. synthesised a mesoporous Li<sub>4</sub>Ti<sub>5</sub>O<sub>12</sub> to the improved electrochemical accessibility over the mesoporosity; the rate capability was considerably enhanced in comparison with that of a commercial Li<sub>4</sub>Ti<sub>5</sub>O<sub>12</sub> sample.

### 2.3.2 Supercapacitor

A supercapacitor, also termed an electrochemical capacitor, is an advanced energy storage system that has fast energy delivery, short charging duration, high power density, long durability and an infinite cycling lifespan. [126] Therefore, many ongoing studies are focusing on improving the energy density of supercapacitors.

Supercapacitors contain electrode materials, separators and electrolytes [127, 128] as shown in Figure 2.7.

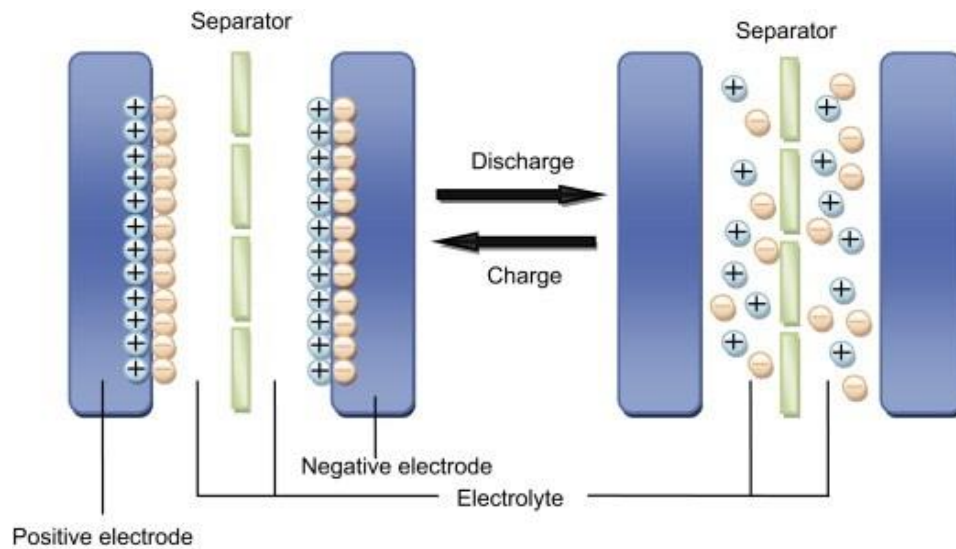


**Figure 2.7: Diagram of supercapacitor**

Generally, the mechanism of energy storage is dependent on one of two types of supercapacitors. First is the double-layer supercapacitor and the second is the redox supercapacitor (pseudo supercapacitor). In the first, the charge is stored in the electrical double layer of each electrode, while in the second, a reversible redox reaction occurs between the electrode and electrolyte.

Carbon-based materials are often employed as electrode materials of double-layer capacitors because of their unique properties, including relatively high surface area and conductivity. However, using the entire surface area is not possible, resulting in low capacitance.

Redox supercapacitors possess high energy density compared with double-layer capacitors. Metal oxides, such as iron oxide, NiO, Co<sub>3</sub>O<sub>4</sub> and ferrite, act as effective electrode materials owing to their natural abundance, environmental friendliness and theoretical specific capacitance. [126, 129]

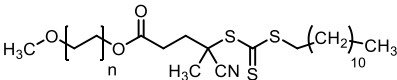
Many studies have reported the preparation of mesoporous metal oxides as electrode materials. Vettrano et al. studied the electrochemistry of ordered amorphous mesoporous TiO<sub>2</sub>, Nb<sub>2</sub>O<sub>5</sub> and Ta<sub>2</sub>O<sub>5</sub> and found that only mesoporous TiO<sub>2</sub> showed reversible redox behaviour. [121] In another study, crystals of hierarchical mesoporous V<sub>2</sub>O<sub>5</sub> were synthesised, demonstrating a large capacitance of 225 F g<sup>-1</sup>. [121] Ordered mesoporous NiO films showed high specific capacitance with 590 F g<sup>-1</sup>. [121] Manganese oxides have also been used widely as supercapacitor materials. Three types of porous MnO<sub>2</sub> (ordered mesoporous b-MnO<sub>2</sub>, disordered mesoporous g-MnO<sub>2</sub> and disordered porous a-MnO<sub>2</sub>) were prepared. Ordered mesoporous b-MnO<sub>2</sub> showed the best rate capability owing to its ordered mesostructure. [121]

## Chapter 3: Techniques Used

### 3.1 Materials and Chemicals

The materials and chemicals utilised in this study for synthesising poly (styrene-block-acrylic acid-block-ethylene glycol) (PS-b-PAA-b-PEG) triblock copolymer and mesoporous NiO are summarised in Table 3.1.

**Table 3.1: Chemicals/Materials used to synthesise copolymer and mesoporous NiO**

| Materials/Chemicals  | Formula   | Purity      | Supplier           |
|--|---|-------------|--------------------|
| 1,4-Dioxane  | C <sub>4</sub> H <sub>8</sub> O <sub>2</sub>  | ≥ 98.8%     | Wako Pure Chemical |
| 2,2'-Azobis (2,4-dimethylvaleronitrile)  | C <sub>14</sub> H <sub>24</sub> N <sub>4</sub>  | ≥ 95.0%     | Wako Pure Chemical |
| 2,2'-Azobis (2-methylpropionitrile)  | (CH <sub>3</sub> ) <sub>2</sub> C(CN)N=NC(CH <sub>3</sub> ) <sub>2</sub> CN                                 | ≥ 98.0%     | Wako Pure Chemical |
| 4 Å Molecular sieves   | Na <sub>12</sub> [(AlO <sub>2</sub> ) <sub>12</sub> (SiO <sub>2</sub> ) <sub>12</sub> ] · xH <sub>2</sub> O | N/A         | Sigma-Aldrich      |
| Acryl acid   | C <sub>3</sub> H <sub>4</sub> O <sub>2</sub>  | ≥ 98.0%     | Wako Pure Chemical |
| Ethanol  | C <sub>2</sub> H <sub>6</sub> O   | 99.99%      | Sigma-Aldrich      |
| Methanol   | CH <sub>3</sub> OH  | 99.99%      | Sigma-Aldrich      |
| Milli-Q Water  | H <sub>2</sub> O  | 5 ppb (TOC) |                    |
| Nickel (II) nitrate hexahydrate  | Ni(NO <sub>3</sub> ) <sub>2</sub> · 6H <sub>2</sub> O   | 98%         | Sigma-Aldrich      |
| Poly (ethylene glycol) methylether (4-cyano-4-pentanoate dodecyl trithiocarbonate) |                         | N/A         | Sigma-Aldrich      |
| Styrene  | C <sub>8</sub> H <sub>8</sub>   | ≥ 99.0%     | Wako Pure Chemical |

## 3.2 Experimental Procedure

The framework for this study contains an optimised synthesis of the designed materials. The structural and physical characterisation follows.

## 3.3 Preparation Approaches

In the present study, the soft-templating method was applied to synthesise mesoporous NiO by using PS-*b*-PAA-*b*-PEG triblock copolymer prepared in National Institute for Materials Science labs.

The effects of nickel precursor concentration, calcination temperature, time and pH were investigated to determine the optimal condition for accomplishing well-defined mesoporous NiO.

### 3.3.1 Preparation of soft template

Polymerisation is the process of chemically linking monomer molecules together in a chemical reaction to form three-dimensional networks or polymer chains. Commonly, polymerisation occurs with several reaction mechanisms, depending on the functional groups in the reacting compounds and their inherent steric effects. Further, the polymers that repeat the same monomer, as shown in the following equation, are termed homopolymers:



By contrast, polymers containing more than one molecule, as illustrated in the following equation, are termed copolymers:



The soft template should be a copolymer because the copolymer should contain a hydrophilic polymer, which must interact with precursors, and a hydrophobic polymer, which works as the SDA.

In this work, a triblock copolymer (i.e., PS-b-PAA-b-PEG) was successfully synthesised containing acrylic acid, which possesses a negative charge. In this copolymer, PS polymer works as the SDA and possess a long chain to enlarge the pores, whereas PAA acts as the reaction site for the metal ions owing to its strong electrostatic interaction with positively charged metal ions. Additionally, the acrylic acid molecules in PAA work as template molecules for the formation of mesoporous NiO. The PEG polymer acts as stabiliser for the micelles formed in the solution.

### **3.3.2 Synthesis mesoporous NiO by soft-templating method**

In the soft-templating method, precursors condense around templates or SDAs that can be supramolecular aggregations of organic molecules or solid structures to form pore structures after removing the SDAs. Regarding control of the phase diagram shape, porosity and pore sizes, the synthesis of mesoporous materials should be adapted according to the nature of the materials, a fraction of concentration between the SDAs and precursors, the pH of the solution and the temperature. Generally, choosing the precursors and synthetic conditions could be validated by the following general considerations:

1. Interactions between inorganic and template materials should be established as a favourable interaction if possible. In this case, to form ordered mesostructured material bonds between the template and precursors, a Coulomb interaction and/or hydrogen bond is needed. When the interaction between these materials is insufficient, there may be a tendency for phase separation. In this case, the material choice should depend on the nature of the materials because some materials possess high tendency to build a stable structure with high lattice energy, such as metals, while others favour amorphous networks, such as silicon. [67, 74, 75]
2. Inorganic species must possess a satisfactorily elevated tendency to condense and form frameworks under synthetic conditions, such as pH, temperature, concentration and time. However, these structures could collapse once the template is removed. [67, 76]
3. Removal of the template should be possible without structural collapse. One popular method for template removal is calcination. However, if the framework is not redox stable, calcination would result in reduction/reoxidation. In this case, the template

hydrocarbon chain could act as a reducing agent and oxygen may not reach the pores. As a result, the pores might be empty, oxygen may penetrate and reoxidation can occur, which would result in a loss of framework structure. This problem can be solved by choosing the appropriate removal process according to the nature of the framework compositions and templates. For example, template removal can be achieved by different processes, such as ozone treatment and H<sub>2</sub>SO<sub>4</sub> treatment. [67, 77-79]

4. Many ordered porous structures with amorphous wall structures can be embedded with nanocrystalline particles in an amorphous matrix. Under high thermal treatment, problems could occur even for redox stable materials, if thermally induced crystallisation of the wall occurs. Hence, the crystallinity of the walls may not be compatible with the porous structures because in many cases curvatures do not form porous structures. In this case, the recrystallisation of the wall could affect the porous structure, resulting in failure of pore formation. [6, 67, 80]

In this study, mesoporous NiO was prepared utilising a PS-*b*-PAA-*b*-PEG triblock copolymer as a soft template to synthesise a large average pore size.

### **3.4 Characterisation and Measurement Methods**

Numerous characterisation techniques are used to investigate porous NiO and poly (styrene-*block*-acrylic acid-*block*-ethylene glycol) block copolymers. Individually, they do not provide sufficient contribution to aspects such as the determination of the structure, morphology, surface features and porosity. However, combining them can yield massive information about the materials used and synthesised.

The equipment used for characterisation belongs to the Institute for Superconducting and Electronic Materials (ISEM), Intelligent Polymer Research Institute under the Australian Institute for Innovative Materials, University of Wollongong, and National Institute for Materials Science in Japan.



### 3.4.1 X-ray diffraction

XRD is considered the leading technique to determine the structural characterisation of the materials. Generally, the x-rays are diffracted by the atoms of materials into several specific directions.

X-rays can be generated by a high-energy beam of electrons accelerated using an elevated electric field to a copper anode inside an x-ray tube. The x-ray tube is designed with a small window that possesses some special properties, including requiring limited attention as regards the spectrum and maintaining the vacuum seal required for the x-ray, to allow the x-ray spectrum to exist in the tube and irradiate the materials outside the x-ray tube.

The x-ray waves are scattered from the target materials. Regular arrays of atoms (crystals) scatter the x-ray in a unique pattern, indicating the nature of the material. In addition, Bragg's law defines the diffraction condition from planes with spacing ( $d$ ):

$$2d\sin\theta = n\lambda \quad (3.3)$$

Here,  $d$  is the distance between diffracting plans,  $n$  is an integer number,  $\lambda$  is the wavelength of the incident x-ray beam and  $\theta$  is the angle of the incident x-ray beam reflected from the faces of the crystal. In addition, the crystal size can be calculated from the broadening of the peaks according to the Scherrer equation:

$$L = \frac{0.9 \times \lambda}{B \times \cos\theta} \quad (3.4)$$

where  $L$  is crystallite size,  $\lambda$  is 1.5418 Å and is the peak full width at half maximum (FWHM) in radians.

In this study, a GBC MMA diffractometer in ISEM was used, where the powder of mesoporous NiO was loaded on a holder and the holder was placed in the device.

### 3.4.2 Scanning electron microscopy

The SEM technique is one of the best characterisation techniques for specification of the surface topography and composition of the materials. Generally, in SEM, the surface of

materials is scanned with high-energy electrons generated from a tungsten or La B6 gun; these electrons interact with the atoms of the samples resulting in signals that contain information about the surface of the sample. These signals may be secondary electrons, back-scattered electrons, characteristic x-rays, light specimen currents or transmitted electrons, and special detectors are available for each of these.

In this work, the morphologies and structures of the samples were characterised using a scanning electron microscope (JEOL 7500) in ISEM.

### **3.4.3 Transmission electron microscopy**

This technique is considered sophisticated, since it is capable of observing the sample's morphology, lattice spacing and crystal orientation. Ordinarily, TEM images of samples depend on a high-energy electron beam that interacts with, and penetrates, the ultra-thin specimen. In addition, selected area electron diffraction is considered one of the best techniques utilised inside the transmission electron microscope to specify whether the sample is amorphous (diffuse rings), crystalline (bright spots) or polyanocrystalline (small spots making up rings, each spot arising from Bragg reflection from an individual crystallite).

Generally, the electrons used in TEM to interact with the samples are extracted from the tungsten filament or lanthanum hexaboride by thermionic or field electron emission into a vacuum under high voltage (typically 100-400 kV). Subsequently, a group of magnetic lenses inside the transmission electron microscope allow formation of an electron probe with the desired size and location for later interaction with the samples. The design of the TEM specimen stage possesses airlocks to allow insertion of the specimen holder into the vacuum with minimum boost in pressure in other areas of the microscope. A thin carbon film, holey carbon or lacey carbon are usually utilised as the support to spatially arrange the samples; these supports are commonly attached with a thin mesh metal grid with a typical mesh spacing of 50–200 nm. This grid with the sample is hung on the sample holder. For TEM, the microscope utilised in this thesis was a JEOL ARM-200F to specify the crystalline and morphology of the samples using the lacey carbon grid.

#### **3.4.4 Thermogravimetric analysis**

The TGA technique is used to provide complementary and supplementary characterisation information of the samples. TGA measures the amount and rate of change in the mass of a sample as a function of temperature or time in a controlled atmosphere. This method can analyse the materials, depending on either mass loss or gain due to decomposition, oxidation or loss of volatiles. In this study, TGA was used to examine the change in weight during the copolymer calcination. TGA was accomplished in air atmosphere utilising a Mettler Toledo TGA/DTA851 thermal analyser in ISEM.

#### **3.4.5 Nitrogen adsorption**

This method characterises porous materials. In this method, adsorbate materials, including nitrogen, argon and krypton, attach to the surface of the adsorbent at specific temperatures. For example, for nitrogen, the temperature is 77K, which is the boiling temperature of nitrogen gas. If there is no interaction between the adsorbate and adsorbent, the process is physisorption and the interaction depends on the van der Waals force. Otherwise, it is chemisorption.

The uptake of gases can be measured in close volume. The weight of the porous materials increases and the pressure of the gas decreases to arrive at the equilibrium point. Subsequently, the amount of the adsorbed gas can be calculated by using the ideal gas law at a constant temperature and volume. The amount of the gas adsorbed ( $n$ ) is proportional to many factors, including the nature of the materials, temperature ( $T$ ), volume ( $V$ ) and pressure ( $P$ ). Here,  $n$  is a function of pressure at constant  $T$  and  $V$ . Relative pressure ( $P/P_0$ ) is applied if the temperature is below the critical temperature of the gas. Then, the amount of the adsorbed gas ( $n$ ) is plotted versus  $p/p_0$ , termed the sorption isotherm.

The sorption isotherm data are analysed to obtain information about the surface area and porosity. This analysis has many modules, including BET and Barrett–Joyner–Halenda (BJH).

The BET method is used to calculate the surface area of the mesoporous materials. The BET equation is:

$$\frac{(P/P_o)}{V_a(1-P/P_o)} = \frac{1}{V_m} + (P/P_o) \frac{(C-1)}{V_m C} \quad (3.5)$$

where  $V_a$  is the volume adsorbed,  $V_m$  is the monolayer volume and  $C$  is the BET constant. Plotting the left side of the BET equation with  $P/P_o$  results in easily calculating  $C$  from the slope  $\frac{(C-1)}{V_m C}$  and  $V_m$  from the intercept  $\frac{1}{V_m}$ . Next, the surface area ( $A$ ) of 1 g of solid can be calculated from:

$$A = NmAmNav \quad (3.6)$$

where  $Nm$  is the amount of adsorbate per gram of adsorbent,  $Am$  is the average area occupied by a molecule in the completed monolayer and  $Nav$  is the Avogadro's constant. If the volume of gas reduces (reduced to STP),  $V_m$  can be used instead, and the equation becomes:

$$A = \frac{V_m}{22414} AmNav \times 10^{-20} \quad (3.7)$$

where  $A$  is in  $m^2/g$ , and  $Am$  is in  $\text{\AA}^2/\text{molecule}$  units (e.g.,  $16.2 \text{\AA}^2$  for nitrogen at 77k).

To calculate the pore sizes, the BJH module is considered the common method. This model is constructed by the Kelvin equation and is corrected for multilayer adsorption utilising statistical film thickness.

$$Rp = Rk + t \quad (3.8)$$

where  $R_p$  is pore radius,  $R_k$  is Kelvin radius and  $t$  is the statistical thickness.

The Kelvin radius can be calculated from the equation:

$$Rk = \frac{-2\gamma V_l}{RT \ln(p/p_o)} \quad (3.9)$$

where,  $\gamma$  is surface tension for the adsorbate and  $V_l$  is the molar volume. In the case of nitrogen, the equation is reduced to:

$$Rk = \frac{-4.14}{\log(p/p_o)} \quad (3.10)$$

Here,  $t$  can be calculated from the standard isotherm (t-plot).

However, this method does not take into account the influence of solid–fluid interactions on capillary condensation. Hence, it underestimates the real pore size.

The Gurvich module is proposed to calculate the pore diameter ( $D$ ) using the equation:

$$D = 4V_{.4}/A \quad (3.11)$$

where  $V_{.4}$  is the volume adsorbed at  $P/P_0 = .4$  and  $A$  is the surface area calculated by the BET module.

In this thesis, nitrogen ( $N_2$ ) adsorption–desorption measurements were performed using a BET Nova 1000 at 77 K. The specific surface areas were calculated using the multipoint BET method at a relative pressure ( $P/P_0$ ) range of 0.05 to 0.30, while the total pore volumes were calculated by the BJH method. Prior to the BET measurements, the samples were degassed under vacuum at 100 °C overnight.

#### **3.4.6 Nuclear magnetic resonance spectroscopy**

NMR spectroscopy is a technique used to obtain the structure, dynamics, reaction state and functional groups contained by a chemical system in either solid or liquid state. Generally, a magnetic field is applied on the samples that possess isotopes with magnetic nuclei, including  $^{13}C$  and  $^1H$ , with a nuclear spin of  $1/2$ . Thus, the excitation of the nuclei in the sample is proportional to the strength of the magnetic field and radio frequency applied with radio waves re-emitted from each nuclei within the magnetic resonance, which are received with sensitive radio detectors as NMR signals. Finally, the chemical structure of the sample can be determined by analysing the NMR spectrum. In this thesis,  $^1H$  NMR was performed using a Bruker DRX-500 spectrometer to specify the chemical structure of PAA71-b-PEG46 in DMSO- $d_6$  at room temperature and PS402-b-PAA71-b-PEG46 in DMF- $d_7$  at 120 °C.

#### **3.4.7 Gel permeation chromatography**

The GPC is a wide separation technique used for separation of polymers, plastics and resins. As a subtype of size exclusion chromatography, the separation of the molecules in GPC is based mainly on size. The sample of interest, of which a small quantity is used, is

partitioned between the porous beads on the stationary phase and the eluent (mobile phase) and separated according to component size. Therefore, it is important to consider the molecular weights of the components of the samples. Dispersity (D), as well as viscosity molecular weight (Mv), can be determined by GPC for polymers and on other data; we can determine the number-average molecular weight (Mn), weight average molecular weight (Mw) and size average molecular weight (Mz).

In this thesis, the GPC measurement was obtained for PAA<sub>71</sub>-b-PEG<sub>46</sub> using a Tosoh RI-8020 refractive index detector equipped with a Shodex 7.0 µm beads size GF-7M HQ column (exclusion limit ~ 107) working at 40 °C within a flow rate of 0.6 mL/min. The GPC measurement for PS<sub>402</sub>-b-PAA<sub>71</sub>-b-PEG<sub>46</sub> was achieved utilising a Shodex DS-4 pump and an RI-101 refractive index detector utilising Shodex one KF-805L and three KF803L columns connected in series.

### 3.4.8 Measurement of zeta potential

Zeta potential ( $\zeta$ ) is a scientific term for electrokinetic potential in colloidal dispersions and is a stability indicator. Generally, the zeta potential of suspended particles can be measured by electrophoresis, which is the motion of a charged particle in an electric field. The zeta potential ( $\zeta$ ) is given by the Smolchowski equation as follows:

$$z = \eta\mu/\varepsilon (\kappa a \gg 1) \quad (3.12)$$

Here,  $\varepsilon$  act as the dielectric constant,  $\kappa$  is the Debye–Hückel parameter and  $a$  is the particle radius. The zeta potential is great indicator of the stability of colloidal dispersions. For example, the high zeta potential indicates a high repulsion force between suspended particles, suggesting the particles are stable and cannot form aggregations.

In this thesis, the zeta potential ( $\zeta$ ) was measured using a Malvern Zetasizer Nano ZS at room temperature, and dynamic light scattering (DLS) measurements were achieved utilising a Malvern Zetasizer Nano ZS with a He–Ne laser (4 mW at 633 nm).

## **Chapter 4: Soft-Templated Synthesis of Mesoporous Nickel Oxide Using Poly (styrene-*block*-acrylic acid-*block*-ethylene glycol) Block Copolymers**

In this study, we report the soft-templated preparation of mesoporous nickel oxide using an asymmetric poly (styrene-*block*-acrylic acid-*block*-ethylene glycol) (PS-*b*-PAA-*b*-PEG) triblock copolymer. This block copolymer forms a micelle consisting of a PS core, a PAA shell and a PEG corona in aqueous solutions, which can serve as a soft template.

Specifically, the PS block forms the core of the micelles on the basis of its lower solubility in water. The anionic PAA block interacts with the cationic Ni<sup>2+</sup> ions present in the solution to generate the shell. The PEG block forms the corona of the micelles and stabilises the micelles by preventing secondary aggregation through steric repulsion between the PEG chains. In terms of textural characteristics, the as-synthesised mesoporous NiO exhibits a large average pore size of 35 nm with large specific surface area and pore volume of 97.0 m<sup>2</sup> g<sup>-1</sup> and 0.411 cm<sup>3</sup> g<sup>-1</sup>, respectively. It is expected that the proposed soft-templated strategy can be expanded to other metal oxides/sulphides in the future for applications in gas sensors, catalysis, energy storage and conversion, optoelectronics and biomedical applications.

## 4.1 Introduction

Over the past decades, porous materials have gained significant interest in various applications, such as energy storage and conversion, sensors, catalysis, biomedical and optoelectronics owing to aspects such as their high surface area, large pore volume and porosity and tunable pore size. [31, 130] Among various types of porous materials, mesoporous materials (materials with pore sizes between 2–50 nm) have attracted the most attention owing to their uniform pore size, rich surface chemistry, controllable wall composition and modifiable surface properties. [49, 131] In particular, mesoporous transition metal oxides are highly attractive for a wide range of applications, including chemical, environmental/energy, optics, electronics, medical and biotechnological applications. [9, 104, 105]

In general, mesoporous transition metal oxides are synthesised by using two approaches: hard- and soft-templating methods. [5] In the hard-templating method, suitable metal precursors are first introduced into the pores of mesoporous templates; subsequent heating results in the desired crystalline metal oxides and selective removal of the template generates the mesoporous metal oxide replica. [132] The pore size, wall thickness and topological structure of the resulting mesoporous metal oxide replica can be controlled to some extent by correspondingly changing those of their templates. To date, many different mesoporous metal oxides (including transition metal oxides) have been reported using the hard-templating (nanocasting) method, including  $\text{TiO}_2$ , [133]  $\text{MnO}_2$ , [134, 135]  $\text{Fe}_3\text{O}_4$ , [136]  $\text{Co}_3\text{O}_4$ , [134, 137]  $\text{Al}_2\text{O}_3$ , [138] and  $\text{WO}_{3-x}$ . [139] However, there are some disadvantages associated with the hard-templating method, such as long and complex procedures, difficulty of filling in the mesoporous silica template owing to complex interactions between the silica and filtrated metal ion precursor and the use of strong acids (e.g., hydrofluoric acid) to remove the hard template. [140, 141]

By contrast, soft-templating methods typically employ surfactants or block copolymers. The synthesis of mesoporous metal oxides by the soft-templating method offers many advantages, including lower cost of the template, simpler procedures that can be carried out under mild conditions and tunable pore size and chemical composition. However, these



methods have some drawbacks since their syntheses are often based on complicated so–gel processes as well as the hydrolysis and polymerisation of transitional metal species, which are difficult to control. Further, the resulting mesoporous oxide products tend to exhibit amorphous or semicrystalline walls and poor thermal stability. Triblock copolymers have previously been employed as soft templates to synthesise mesoporous transition metal oxides with small pore sizes. [101, 142] For instance, Yang et al. have reported the synthesis of mesoporous TiO<sub>2</sub> with an average pore size smaller than 10 nm by using the PEO-*b*-PPO-*b*-PEO type block copolymer. [143] However, mesoporous materials with such small pores may have limited applications compared with those with larger pores because they may not be able to accommodate large guest species or molecules.

Recently, many efforts have been made to enlarge the pore size of mesoporous materials. The utilisation of block copolymers that possess long hydrophobic block could overcome this challenge because the pore size strongly relies on hydrophobic block length of the micelle template. Previously, our group reported the use of high molecular weight diblock copolymers, such as polystyrene-*block*-poly (ethylene oxide) (PS-*b*-PEO) as soft templates for the preparation of mesoporous materials with large pore sizes. [101, 144, 145] Further, we synthesised mesoporous nickel ferrite and ferrite with large pore sizes by using poly (styrene-*block*-acrylic acid-*block*-ethylene glycol) (PS-*b*-PAA-*b*-PEG) triblock copolymer containing acrylic acid (negatively charged in alkaline solutions). [146]

Among various metal oxides, nickel oxide (NiO), a wide bandgap (3.6-4.0 eV) *p*-type semiconductor has gained significant attention because of its exciting intrinsic properties, such as electrochromic, antiferromagnetic and high capacitive properties. [142, 147] In addition, NiO can be utilised in a wide range of applications, including electrochromic display devices, smart windows, active optical fibres, gas sensors, solar thermal absorbers, catalysis, fuel cell electrodes, supercapacitors and energy storage. [142, 147] To date, many previous reports on mesoporous NiO relied on the use of hard templates, such as SBA-15[141] and KIT-6. Despite some progress, reports on the fabrication of mesoporous NiO using soft templates are still scarce.

In this study, we report the synthesis of mesoporous NiO with a large average pore size of 35 nm by utilising PS-*b*-PAA-*b*-PEG triblock copolymer as a soft template (Figure 4.1). In

aqueous solution, the PS-*b*-PAA-*b*-PEG block polymer forms tri-functional micelles, in which the PS, PAA and PEG blocks act as core, shell and corona, respectively. The effects of nickel precursor amount and calcination temperature were investigated to determine the optimum condition for achieving well-defined mesoporous NiO.

## 4.2 Experimental Section

### 4.2.1 Chemicals

Poly (ethylene glycol) methyl ether (4-cyano-4-pentanoate dodecyl trithiocarbonate) (PEG<sub>46</sub>-CTA,  $M_n = 2,400 \text{ g mol}^{-1}$ ) from Aldrich and 2, 2'-azobis (2, 4-dimethylvaleronitrile) (V-65,  $\geq 95.0\%$ ) from Wako Pure Chemical were used as received without further purification. Acryl acid (AA,  $\geq 98.0\%$ ) and styrene (St,  $\geq 99.0\%$ ) from Wako Pure Chemical were dried with 4 Å molecular sieves and purified by distillation under reduced pressure. 2,2'-Azobis (2-methylpropionitrile) (azobisisobutyronitrile [AIBN];  $\geq 98.0\%$ ) from Wako Pure Chemical was purified by recrystallisation from methanol. 1,4-Dioxane and methanol were dried with 4 Å molecular sieves and purified by distillation. Water was purified using a Millipore Milli-Q system. Nickel (II) nitrate hexahydrate ( $\text{Ni}(\text{NO}_3)_2 \cdot 6\text{H}_2\text{O}$ , 98%) and absolute ethanol ( $\text{C}_2\text{H}_6\text{O}$ , 99.99%) were purchased from Sigma-Aldrich and were used without further purification.

#### 4.2.2 Preparation of PS<sub>402</sub>-*b*-PAA<sub>71</sub>-*b*-PEG<sub>46</sub> triblock copolymer

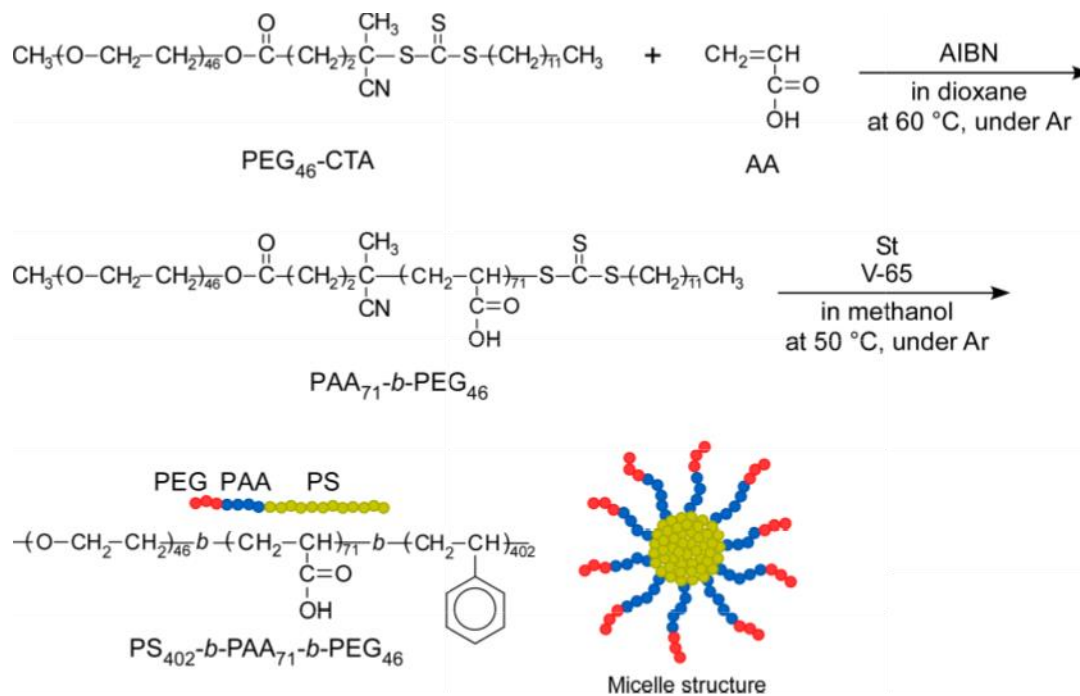


**Figure 4.1: Synthesis route of PS<sub>402</sub>-*b*-PAA<sub>71</sub>-*b*-PEG<sub>46</sub>**

The preparation method of PS<sub>402</sub>-*b*-PAA<sub>71</sub>-*b*-PEG<sub>46</sub> is shown in Figure 4.1. AA (4.95 g, 68.7 mmol), PEG<sub>46</sub>-CTA (1.10 g, 0.458 mmol) and AIBN (30.1 mg, 0.183 mmol) were dissolved in 1, 4-dioxane (70.0 mL). The solution was degassed by purging with argon gas for 30 min. Polymerisation was performed at 60 °C for 15 h. After the reaction, the conversion of AA estimated from <sup>1</sup>H NMR was 40.4%. The reaction mixture was dialysed against pure water for three days. PAA<sub>71</sub>-*b*-PEG<sub>46</sub> was recovered by freeze-drying (2.44 g, 40.4 %). The number-average molecular weight ( $M_n$ (NMR)), degree of polymerisation (DP) of PAA estimated from <sup>1</sup>H NMR and molecular weight distribution ( $M_w/M_n$ ) estimated from GPC were  $7.52 \times 10^3$  g mol<sup>-1</sup>, 71 and 1.41, respectively (Table 4.1).

**Table 4.1: DP,  $M_n$  and  $M_w/M_n$  of PAA<sub>71</sub>-*b*-PEG<sub>46</sub> and PS<sub>402</sub>-*b*-PAA<sub>71</sub>-*b*-PEG<sub>46</sub>**

|   | DP<br>(theory)  | $M_n$<br>(theory)<br>(g/mol) | DP<br>(NMR)     | $M_n$<br>(NMR)<br>(g/mol) | $M_n$<br>(GPC)<br>(g/mol) | $M_w/M_n$ |
|---|-----------------|------------------------------|-----------------|---------------------------|---------------------------|-----------|
| PAA <sub>71</sub> - <i>b</i> -PEG <sub>46</sub> | 61 <sup>a</sup> | 6,770                        | 71 <sup>a</sup> | 7,520                     | 10,300                    | 1.41      |

|   |                  |        |                  |        |         |      |
|---|------------------|--------|------------------|--------|---------|------|
| PS <sub>402</sub> - <i>b</i> -PAA <sub>71</sub> - <i>b</i> -PEG <sub>46</sub> | 276 <sup>b</sup> | 35,500 | 402 <sup>b</sup> | 49,400 | 143,000 | 1.37 |
|---|------------------|--------|------------------|--------|---------|------|

<sup>a</sup>DP of PAA block. <sup>b</sup>DP of PS block.

PAA<sub>71</sub>-*b*-PEG<sub>46</sub> (1.50 g, 0.200 mmol,  $M_n(\text{NMR}) = 7.52 \times 10^3 \text{ g mol}^{-1}$ ,  $M_w/M_n = 1.41$ ), St (10.4 g, 99.8 mmol) and V-65 (24.9 mg, 0.100 mmol) were dissolved in methanol (50.0 mL). The solution was degassed by purging with argon gas for 30 min. Polymerisation was performed at 50 °C for 24 h. After the reaction, the conversion of St estimated from <sup>1</sup>H NMR was 55.2%. The reaction mixture was dialysed against methanol for three days, and then pure water for two days. After the dialysis, the aqueous solution of PS<sub>402</sub>-*b*-PAA<sub>71</sub>-*b*-PEG<sub>46</sub> was recovered (362 mL). The polymer powder was recovered from a part of the aqueous polymer solution (20 mL) by freeze-drying with a yield of 0.355 g. The concentration of the aqueous polymer solution was 17.8 g/L.  $M_n(\text{NMR})$  of PS<sub>402</sub>-*b*-PAA<sub>71</sub>-*b*-PEG<sub>46</sub> and DP(NMR) of PS estimated from <sup>1</sup>H NMR, and  $M_w/M_n$  estimated from GPC were  $4.94 \times 10^4 \text{ g mol}^{-1}$ , 402 and 1.37, respectively (Table 4.1).

### 4.2.3 Synthesis of mesoporous nickel oxide

In a typical procedure, 20 mg of nickel (II) nitrate hexahydrate was first dissolved in 80 µL of ethanol. After perfect dissolution, this solution was added into 2 mL of polymeric micelles solution (5 g L<sup>-1</sup>) under magnetic stirring. After stirring for 1 h, the mixture was dried at 60 °C in an electrical oven. The collected light green powder was then calcined at different temperatures (250–450 °C) with a heating rate of 2 °C min<sup>-1</sup>.

### 4.3 Characterisation

<sup>1</sup>H NMR was obtained using a Bruker DRX-500 spectrometer. GPC measurement for PAA<sub>71</sub>-*b*-PEG<sub>46</sub> was performed using a Tosoh RI-8020 refractive index detector equipped Shodex 7.0 µm beads size GF-7M HQ column (exclusion limit ~ 10<sup>7</sup>) working at 40 °C under a flow rate of 0.6 mL/min. A phosphate buffer (50 mM, pH 9) containing 10 vol% acetonitrile was used as an eluent. The values of  $M_n$  and  $M_w/M_n$  for the polymers were calibrated using standard sodium poly (styrenesulphonate) samples. GPC measurement for PS<sub>402</sub>-*b*-PAA<sub>71</sub>-*b*-PEG<sub>46</sub> was performed using a Shodex DS-4 pump and an RI-101 refractive index detector using Shodex one KF-805L and three KF803L columns connected

in series. Tetrahydrofuran was used as the eluent at a flow rate of 1.0 mL/min at 40 °C.  $M_n$  and  $M_w/M_n$  were calibrated using PS standard samples. Sample solutions were filtered with a 0.2  $\mu\text{m}$  pore size membrane filter. DLS measurements were performed using a Malvern Zetasizer Nano ZS with a He–Ne laser (4 mW at 633 nm) at 25 °C. The hydrodynamic radius ( $R_h$ ) was calculated using the Stokes–Einstein equation,  $R_h = k_B T / (6\pi\eta D)$ , where  $k_B$  is the Boltzmann constant,  $T$  is absolute temperature and  $\eta$  is solvent viscosity. The DLS data were analysed using Malvern Zetasizer software version 7.11. Zeta potential ( $\zeta$ ) was measured using a Malvern Zetasizer Nano ZS at 25 °C.  $\zeta$  was calculated from the electrophoretic mobility ( $\mu$ ) using the Smoluchowski relationship,  $\zeta = \eta\mu/\varepsilon (\kappa a \gg 1)$ , where  $\varepsilon$  is the dielectric constant of the solvent,  $\kappa$  is the Debye–Hückel parameter and  $a$  is particle radius, respectively. TEM observation was performed with a JEOL JEM-2100 operated at an accelerating voltage of 200 kV. The TEM sample was prepared by placing one drop of the aqueous solution on a copper grid coated with a thin film of Formvar. Excess water was blotted using filter paper. The sample was stained by sodium phosphotungstate and dried under vacuum for one day. The morphological observation of the mesoporous NiO was performed through SEM (JEOL JSM-7500FA) and TEM (JEOL JEM-2100). The phase composition and crystal structures of the samples were analysed by XRD (GBC MMA XRD) with Cu-K $\alpha$  (1.54 Å) in the  $2\theta$  range of 10 to 80°. Nitrogen (N<sub>2</sub>) adsorption–desorption measurements were performed using a BET Nova 1000 at 77 K. The specific surface areas were calculated using the multipoint BET method at a relative pressure ( $P/P_0$ ) range of 0.05 to 0.30, while the total pore volumes were calculated by the BJH method. Prior to the BET measurements, the samples were degassed under vacuum at 100 °C overnight. Finally, TGA was carried out using a Mettler Toledo TGA/DTA851 thermal analyser apparatus with a heating rate of 10 °C min<sup>-1</sup> in air atmosphere.

## 4.4 Result and Discussion

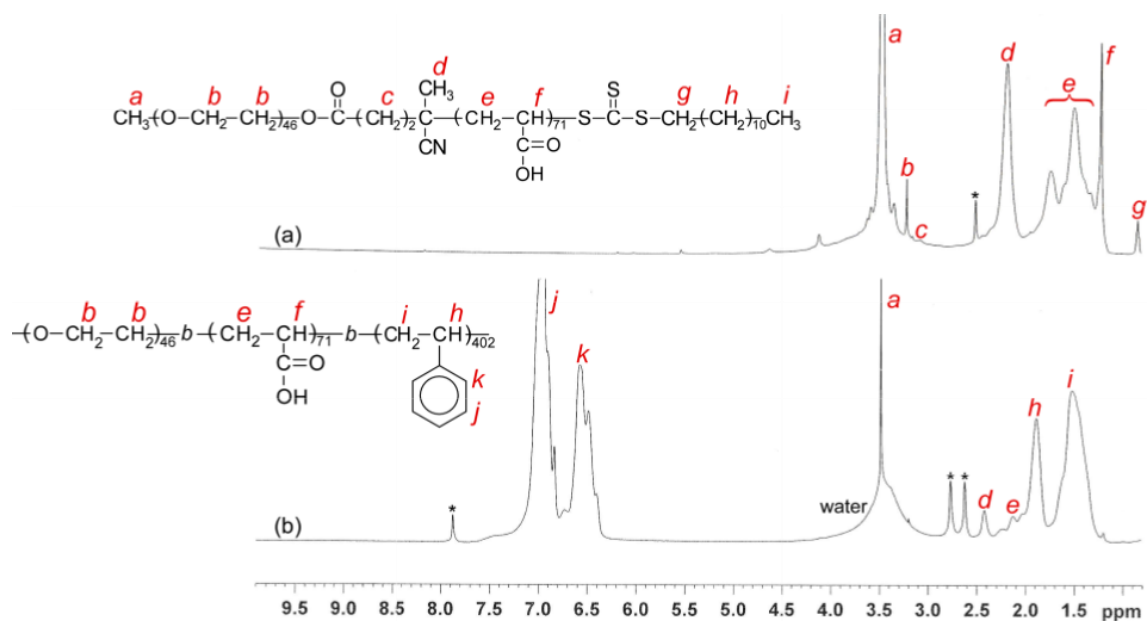


**Figure 4.2:**  $^1\text{H}$  NMR spectra of (a) PAA<sub>71</sub>-*b*-PEG<sub>46</sub> in DMSO-*d*<sub>6</sub> at room temperature and (b) PS<sub>402</sub>-*b*-PAA<sub>71</sub>-*b*-PEG<sub>46</sub> in DMF-*d*<sub>7</sub> at 120 °C

The DP (NMR) for PAA was determined from the integral intensity ratio of the peaks at 3.5 (a) and 1.1–1.9 ppm (e+f) (Figure 4.2a). The DP (NMR) for PS was determined from the integral intensity ratio of the peaks at 1.2–2.5 (d+e+h+i) and 6.3–7.2 ppm (j+k) (Figure 4.2b). The  $M_n(\text{GPC})$  values for PEG<sub>46</sub>-*b*-PAA<sub>71</sub> and PS<sub>402</sub>-*b*-PAA<sub>71</sub>-*b*-PEG<sub>46</sub> were  $1.03 \times 10^4$  and  $1.43 \times 10^5 \text{ g mol}^{-1}$ , respectively (Figure 4.3).

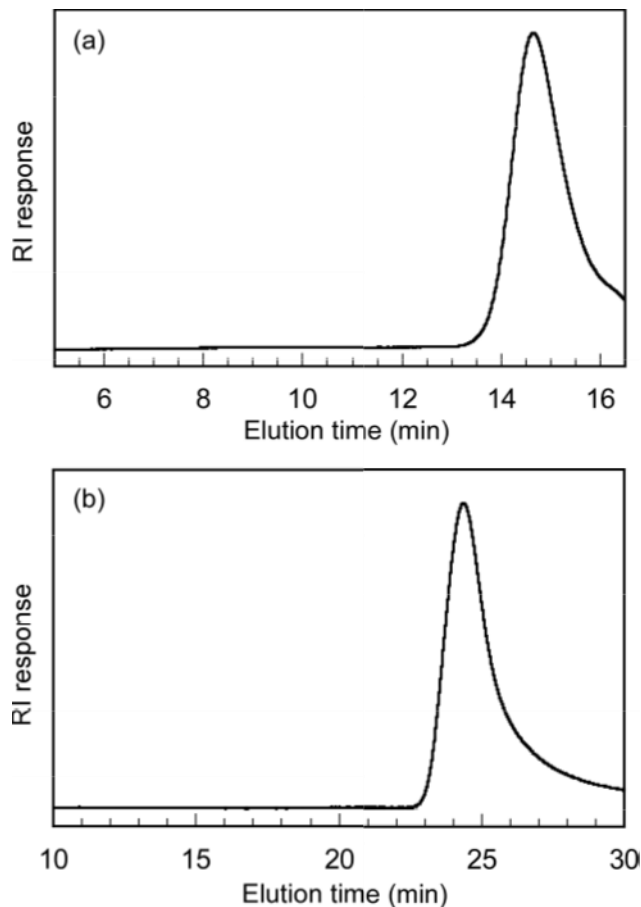


**Figure 4.3: GPC elution curves of (a) PAA<sub>71</sub>-*b*-PEG<sub>46</sub> using phosphate buffer (50 mM, pH 9) containing 10 vol % acetonitrile and (b) PS<sub>402</sub>-*b*-PAA<sub>71</sub>-*b*-PEG<sub>46</sub> using tetrahydrofuran as an eluent**

$M_w/M_n$  estimated from GPC were relatively narrow below 1.5 (Table 4.1). Theoretical degree of polymerisation (DP (theory)) and theoretical number-average molecular weight ( $M_n$ (theory)) were calculated using the following equations:

$$DP(\text{theory}) = \frac{[M]_0}{[CTA]_0} \times \frac{P}{100} \quad (4.1)$$

$$M_n(\text{theory}) = DP(\text{theory}) \times MW + MW_{CTA} \quad (4.2)$$

where  $[M]_0$  is the initial monomer concentration,  $[CTA]_0$  is the initial chain transfer agent (CTA) concentration,  $p$  is monomer conversion estimated from  $^1\text{H}$  NMR measurements,  $MW$  is the molecular weight of monomer and  $MW_{CTA}$  is the molecular weight of CTA.

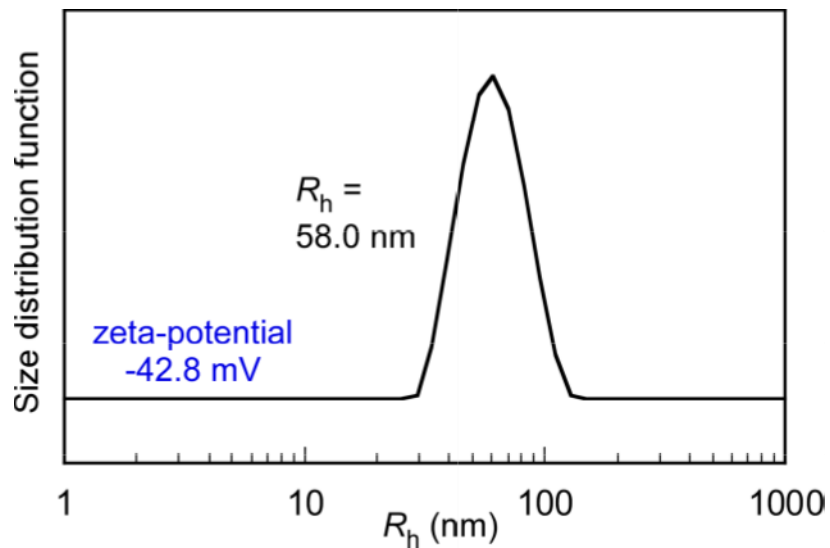


**Figure 4.4: Hydrodynamic radius ( $R_h$ ) distribution of PS<sub>402</sub>-*b*-PAA<sub>71</sub>-*b*-PEG<sub>46</sub> in pure water at pH 5.1**

The values of DP(theory) and  $M_n$ (theory) are listed in Table 4.1. DLS measurements for PS<sub>402</sub>-*b*-PAA<sub>71</sub>-*b*-PEG<sub>46</sub> at polymer concentration ( $C_p$ ) = 0.2 g/L were performed in pure water at pH 5.1 (Figure 4.4). The unimodal distribution with  $R_h = 58.0$  nm can be observed. PAA was ionised in pure water. The zeta potential of PS<sub>402</sub>-*b*-PAA<sub>71</sub>-*b*-PEG<sub>46</sub> in water at pH 5.1 was  $-42.8$  mV, because the pH value of the aqueous solution was 5.1, which is near  $pK_a$  (= 4.35) of AA monomer.

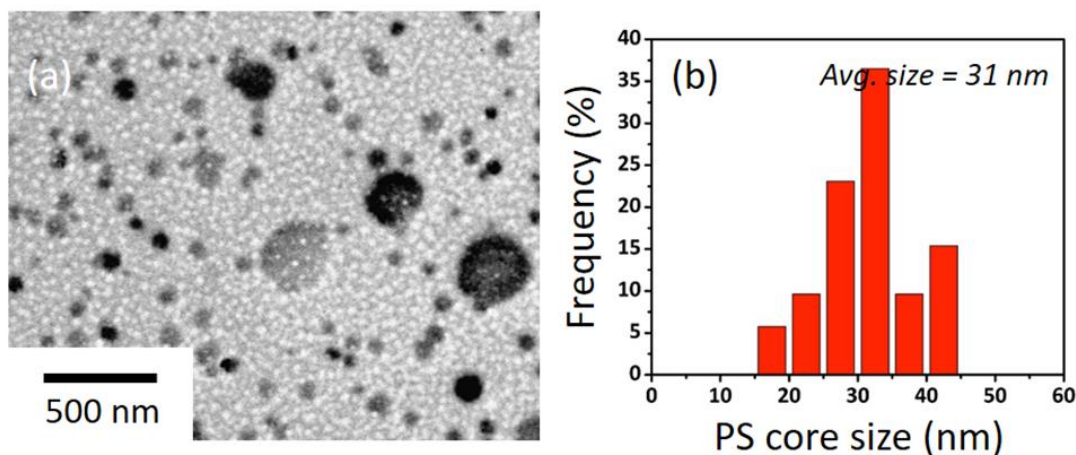


**Figure 4.5: (a) TEM image of PS<sub>402</sub>-*b*-PAA<sub>71</sub>-*b*-PEG<sub>46</sub> in pure water at  $C_p = 0.2$  g L<sup>-1</sup>. (b) Diameter distribution histogram of the polymeric micelles**



TEM observation for PS<sub>402</sub>-*b*-PAA<sub>71</sub>-*b*-PEG<sub>46</sub> in pure water was performed (Figure 4.5a). An average diameter of 31 nm was estimated from TEM (Figure 4.5b), which was different from  $R_h$  (= 58.0 nm) estimated from DLS measurement since the TEM sample was in dried state.

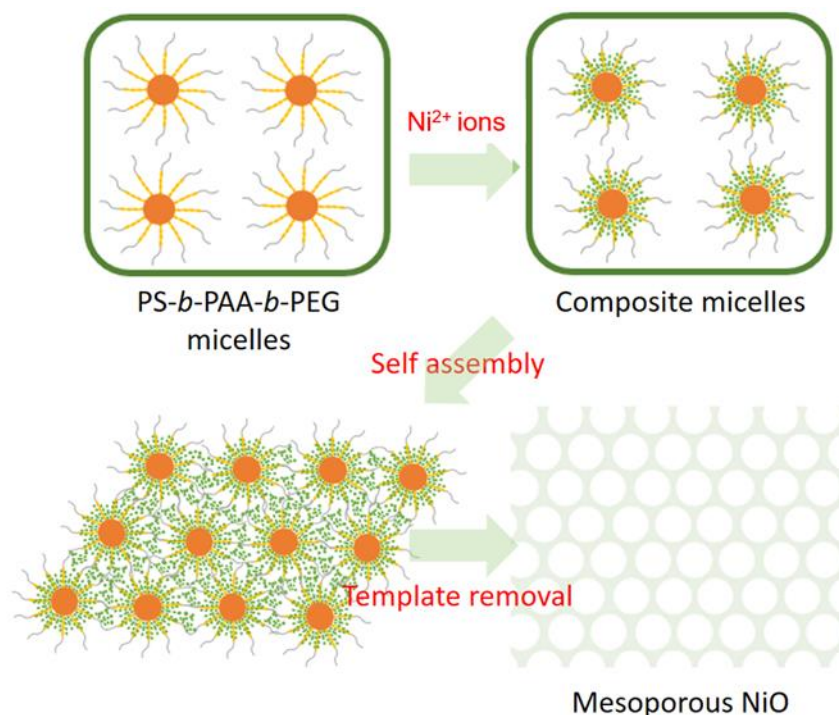


**Figure 4.6: Schematic illustration showing the mechanism of the formation of mesoporous NiO using the PS-*b*-PAA-*b*-PEG triblock copolymer template**

The formation mechanism of the mesoporous NiO using the PS-*b*-PAA-*b*-PEG block copolymer as a soft template is illustrated in Figure 4.6. In the reaction system, the PS block forms the core of the micelles owing to its rigid, glassy structure in water and acts as a pore-forming agent. [146, 148] According to the zeta potential, PAA was negatively charged in the water. After addition of nickel (II) nitrate solution, the pH value was changed to around 4.5. In this pH region, PAA is still negatively charged, where the negatively charged PAA block interacted with the positively charged cationic metal ions and formed the shell. [148] In this study, unlike in our previous study, [112, 149] NaOH solution was not used as additive for controlling the pH in the solution. The PEG block forms the corona, which provides stability for the micelles in the solution to prevent

secondary aggregation and promote the orderly organisation of the particles during assembly of the micelles. The drying of the solution at 60 °C promotes the formation of mesostructured material. Finally, the calcination at high temperatures can lead to cross-linking of the NiO frameworks and simultaneous removal of the polymeric template.

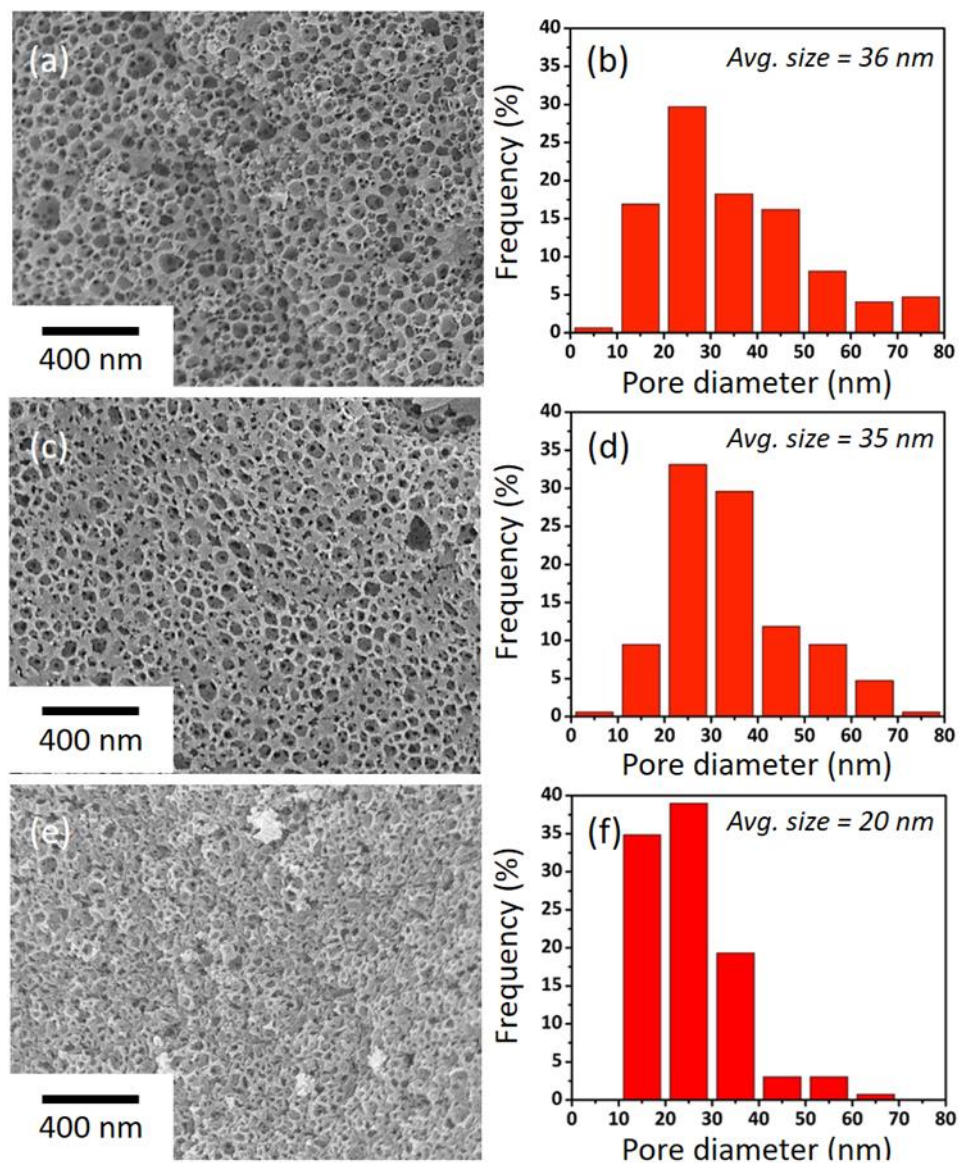


**Figure 4.7:** (a, c, e) SEM images and (b, d, f) the corresponding pore diameter distributions of mesoporous NiO obtained using different amounts of nickel salt: (a) 10 mg (0.0344 mmol), (b) 20 mg (0.0688 mmol) and (c) 30 mg (0.1032 mmol)

To determine the optimised conditions for the synthesis of mesoporous NiO, the effects of using different concentrations of nickel salt were investigated and the corresponding SEM images are given in Figure 4.7. The use of a low amount of nickel precursor (10 mg, 0.0344 mmol) is found to yield mesoporous structures with a large average pore size of around 36 nm, but with very thin walls (thickness of around 6 nm) that have some defects (Figures 4.7a and b). The increase in the amount of the nickel precursor to 20 mg (0.0688 mmol) gives rise to well-defined mesoporous structures with average pore size and wall thickness of 35 nm and 14 nm, respectively (Figures 7c and d). However, excess addition of the nickel salt (30 mg, 0.1032 mmol) results in aggregation of the small crystals, thereby leading to the collapse of the mesopores and the corresponding decrease in surface area (Figures 4.7e and f). Based on these results, the optimum amount of nickel precursor of 20 mg (0.0688 mmol) was used for further experiments.

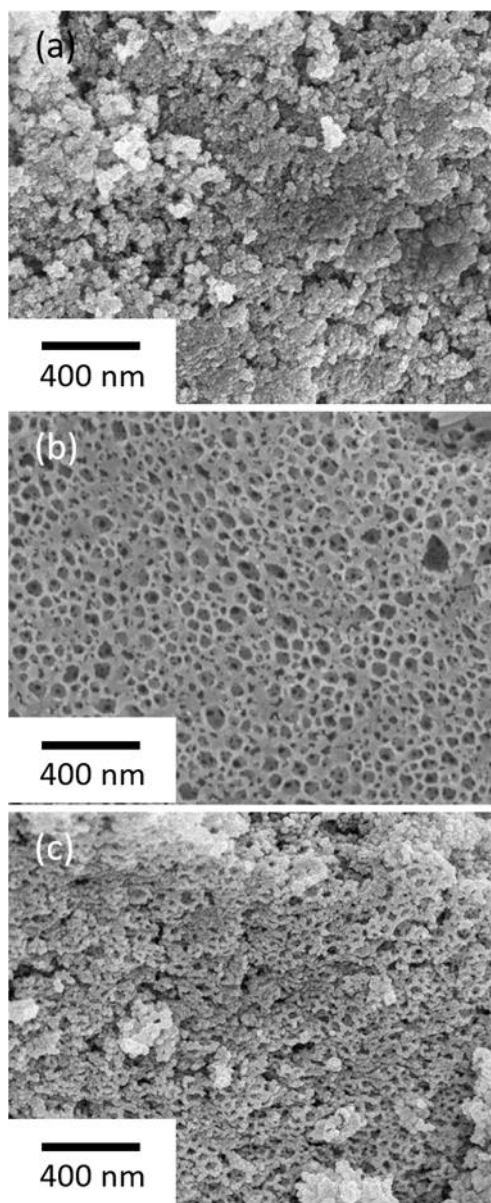


**Figure 4.8: SEM images of the mesoporous NiO obtained at (a) 250 °C, (b) 350 °C and (c) 450 °C**

The effect of the calcination temperature on the morphology of the resulting mesoporous NiO was checked by SEM (Figure 4.8). When the sample is calcined at 250 °C, the mesoporous structure is not observed at all (Figure 4.8a). This is because the temperature is not high enough to remove the carbon components in the PS-*b*-PAA-*b*-PEG block copolymer. In contrast, the increase in calcination temperature to 350 °C leads to the formation of well-defined mesoporous NiO with an average pore size of around 35 nm

(Figure 4.8b). However, raising the calcination temperature further to 450 °C causes the collapse of the mesoporous structures because the higher temperature induced further crystallisation of NiO (Figure 4.8c).

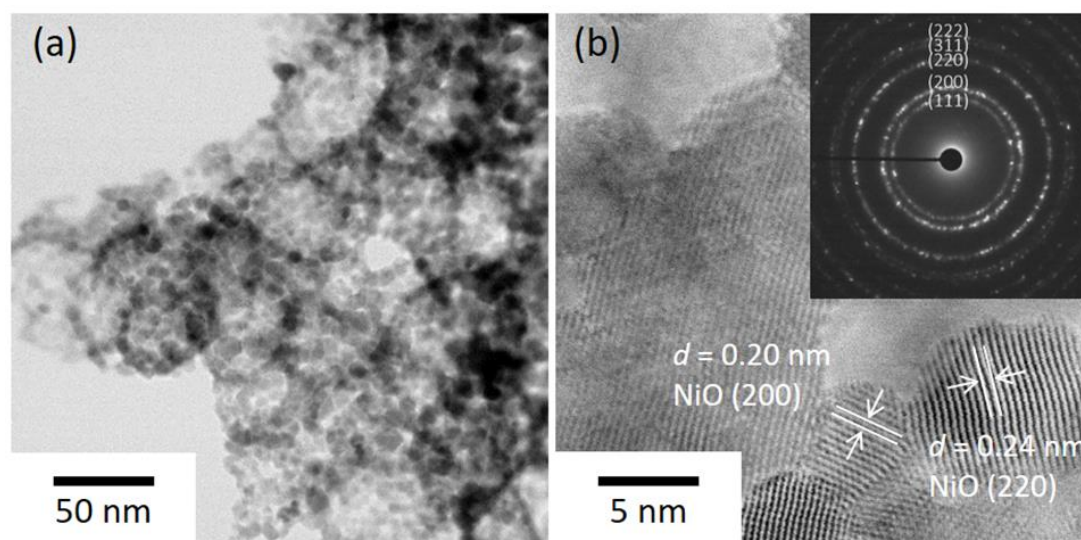


**Figure 4.9: (a) TEM and (b) high-resolution TEM images of mesoporous NiO obtained at an optimised calcination temperature of 350 °C (inset of (b): selected area electron diffraction)**

The TEM image of the mesoporous NiO obtained at an optimum calcination temperature of 350 °C reveals its well-defined mesoporous structure with average pore and grain sizes of 35 nm and 6 nm, respectively (Figure 4.9a). The pore size of mesoporous NiO was slightly larger than the micelle size of block copolymer (Figure 4.5) because the PEG-PAA shell can also contribute to the formation of pores during reaction. The high-resolution TEM image of the mesoporous NiO obtained at 350 °C displays well-defined lattice fringes with  $d$ -spacing of 0.24 nm and 0.20 nm, corresponding to the  $d$ -spacing of NiO(111) and NiO(200), respectively, as shown in Figure 4.10b. The corresponding selected area electron diffraction pattern (Inset of Figure 4.10b) reveals the polycrystalline nature of this mesoporous NiO.

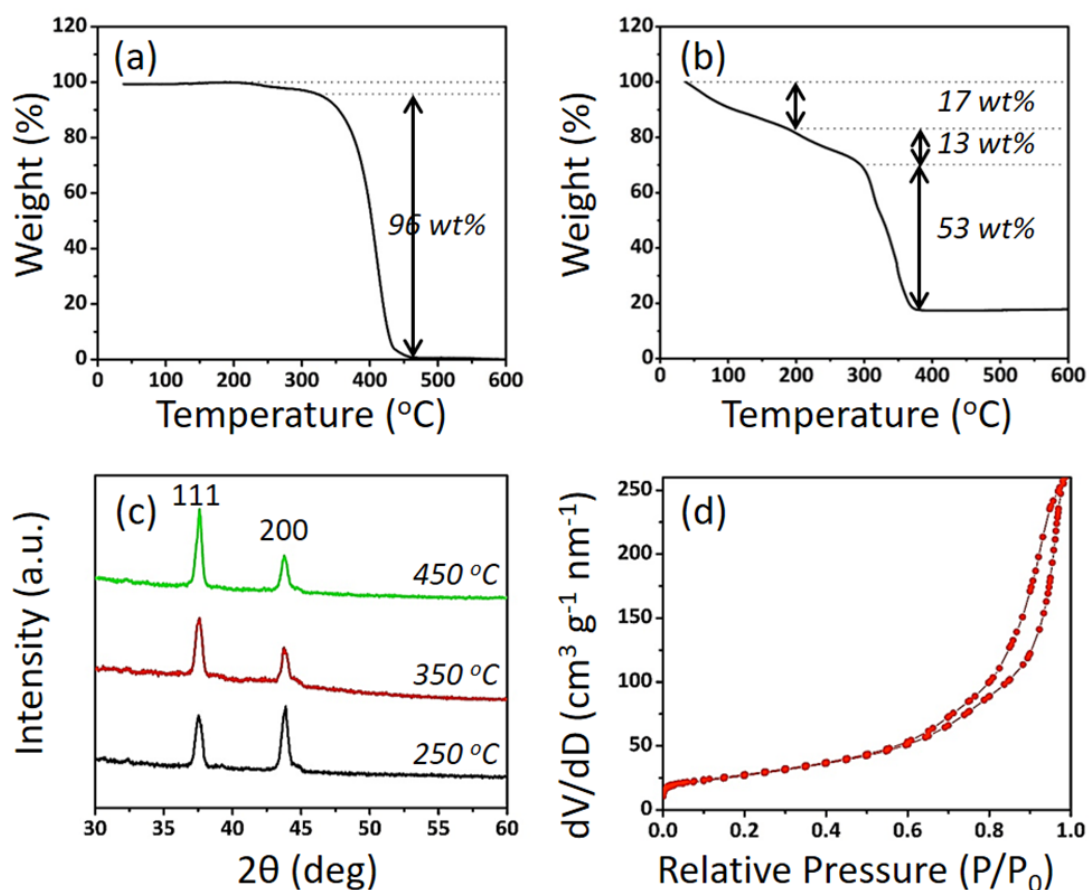


**Figure 4.10:** TG curves of (a) PS-*b*-PAA-*b*-PEG triblock copolymer and (b) PS-*b*-PAA-*b*-PEG micelles (with Ni<sup>2+</sup>). (c) Wide-angle XRD patterns for mesoporous NiO obtained at different calcination temperatures and (d) N<sub>2</sub> adsorption-desorption isotherms of mesoporous NiO obtained at the optimised calcination temperature of 350 °C.

TGA was conducted to analyse the weight changes of pure PS-*b*-PAA-*b*-PEG triblock copolymer and the PS-*b*-PAA-*b*-PEG micelles (containing Ni<sup>2+</sup>) with increasing temperatures. As shown in Figure 4.10a, the block copolymer undergoes a sharp weight loss beginning at around 200 °C and completely burns out at around 450 °C. Conversely, for PS-*b*-PAA-*b*-PEG micelles (containing Ni<sup>2+</sup>), an initial decrease of the TG curve is observed at ~200 °C (~17%), which can be associated with the removal of adsorbed water molecules, whereas the weight loss observed from 200 °C to 370 °C could be attributed to the decomposition of the PS-*b*-PAA-*b*-PEG template, as shown in Figure 4.10b. No further weight loss was observed after 370 °C, indicating the complete removal of the polymeric

template. Therefore, it can be concluded that the calcination process at 350 °C is enough to completely remove the organic template if the applied heating rate is very slow (in our experiment, the heating rate was 2 °C min<sup>-1</sup>). These results are in good agreement with the SEM observations.

The XRD patterns of the mesoporous NiO obtained at different calcination temperatures are shown in Figure 4.10c. The observed diffraction peaks can be indexed to the (111) and (200) planes of face-centred cubic NiO phase (JCPDS No. 01-078-0429). Further, it is evident that the diffraction peaks of the mesoporous NiO become narrower and sharper with increasing calcination temperature. The average crystallite size was calculated from the most intense diffraction peak by using Scherrer's formula:

$$D = 0.94\lambda/(\beta \cos\theta) \quad (4.3)$$

where  $D$  is the average crystallite size,  $\beta$  is the broadening of FWHM of the main intense peak (111) in radian,  $\theta$  is the Bragg angle and  $\lambda$  is the radiation wavelength. Using this equation, the average crystallite sizes of the mesoporous NiO obtained at calcination temperatures of 250 °C, 350 °C and 450 °C are calculated to be 19.5 nm, 27.4 nm and 36.5 nm, respectively. This trend clearly indicates the increase in average crystallite size with increasing calcination temperature.

The XRD pattern of the mesoporous NiO obtained at 250 °C shows the existence of crystalline NiO; however, this temperature is not sufficient to remove the block copolymer template completely, as supported by the TGA data. The increase in calcination temperature of up to 450 °C leads to further improvement in the crystallinity of the mesoporous NiO product, as indicated by the increase in intensity of the NiO(111) peak observed in Figure 4.10b and c. The nitrogen adsorption–desorption isotherm of the mesoporous NiO obtained at an optimum calcination temperature of 350 °C is shown in Figure 4.10d. According to the BET analysis, the specific surface area and pore volume of the mesoporous NiO obtained at 350 °C are 97 m<sup>2</sup> g<sup>-1</sup> and 0.411 cm<sup>3</sup> g<sup>-1</sup>, respectively.

## 4.5 Conclusion

In this study, well-defined mesoporous NiO with large average pore size of 35 nm was successfully synthesised using PS-*b*-PAA-*b*-PEG block copolymer as a soft template followed by its removal at an optimum calcination temperature of 350 °C. In the proposed method, the PS block forms the core of the micelles and functions as a pore-forming agent, whereas the PAA block interacts with cationic Ni ions to form the shell of the micelles owing to its strong electrostatic charge. Further, the PEG block forms the corona of the micelles and provides stability by preventing secondary aggregation before/during micelle assembly. An optimum amount of the nickel precursor is necessary to ensure the formation of well-defined mesoporous NiO. The optimum mesoporous NiO sample exhibits large surface area and pore volume of 97.0 m<sup>2</sup> g<sup>-1</sup> and 0.411 cm<sup>3</sup> g<sup>-1</sup>, respectively. The excellent textural properties of the synthesised mesoporous NiO may enable it to be utilised as high-performance material in catalysis, gas sensors, energy storage and conversion, and biomedical applications. The large surface area and pore volumes of the mesoporous NiO are expected to be beneficial in enhancing its functional performance for a variety of applications, including energy storage and conversion, [44, 150-152] catalysis, [153, 154] gas sensors [155] and biomedical applications. [156] Further, the proposed soft-templating method can be expanded to other metal oxides or sulphides in the future for obtaining mesoporous oxides/sulphides with enhanced textural characteristics and functional performance.

## Acknowledgement

This work was supported by an Australian Research Council Future Fellow (FT150100479) and JSPS KAKENHI (Grant Numbers 17H05393 and 17 K19044). Yusuf Valentino Kaneti is an overseas researcher under Postdoctoral Fellowship from the Japanese Society for the Promotion of Science (JSPS). This work was also supported by the Deanship of Scientific Research, King Abdulaziz University (KEP-7-130-39).



## Chapter 5: Conclusion

### 5.1 Conclusion

In the present study, poly (styrene-block-acrylic acid-block-ethylene glycol) block copolymers prepared in the laboratory with long hydrophobic block are successfully used as a soft template for synthesis mesoporous NiO with large average pore size of 35 nm and the template is subsequently removed at an optimum calcination temperature of 350 °C. In the proposed method, the copolymer utilised forms tri-functional micelles in an aqueous solution, in which the PS block (hydrophilic part) forms the core of the micelles and functions as a pore-forming agent, while the PAA block interacts with cationic Ni ions to form the shell of the micelles owing to its strong electrostatic charge. Further, the PEG block forms the corona of the micelles and provides stability by preventing secondary aggregation before and during micelle assembly. By precisely determining the experimental parameters, including concentrations of materials, pH, temperature and time, the optimum well-defined mesoporous NiO was obtained with large surface area and pore volume of 97.0 m<sup>2</sup> g<sup>-1</sup> and 0.411 cm<sup>3</sup> g<sup>-1</sup>, respectively.

The synthesised mesoporous NiO, which has various excellent properties, including d-shell electrons confined to nanosized walls, redox active internal surfaces, large average pore size and connected pore networks, could be used as a high-performance material in catalysis, gas sensors, energy storage and conversion, and biomedical applications. The large surface area and pore volumes of the mesoporous NiO are expected to be beneficial in enhancing its functional performance for a variety of applications, including energy storage and conversion, catalysis, gas sensors and biomedical applications. In addition, the proposed soft-templating method can be generalised for other metal oxides or sulphides in the future to obtain further mesoporous oxides or sulphides with enhanced textural characteristics and functional performance.

## References

1. Hillmyer, M.A., *Nanoporous materials from block copolymer precursors*, in *Block copolymers II*. 2005, Springer. p. 137-181.
2. Lu, G. and X. Zhao, *Nanoporous materials—an overview*, in *Nanoporous materials: science and engineering*. 2004, World Scientific. p. 1-13.
3. Suib, S.L., *A review of recent developments of mesoporous materials*. Chemical Record, 2017. **17**(12): p. 1169-1183.
4. Max, L.G. and Z.X. Song, *Nanoporous materials: science and engineering*. Vol. 4. 2004: World Scientific.
5. Malgras, V., et al., *Templated synthesis for nanoarchitected porous materials*. Bulletin of the Chemical Society of Japan, 2015. **88**(9): p. 1171-1200.
6. Dahal, N., I.A. Ibarra, and S.M. Humphrey, *High surface area mesoporous Co<sub>3</sub>O<sub>4</sub> from a direct soft template route*. Journal of Materials Chemistry, 2012. **22**(25): p. 12675-12681.
7. Ariga, K., et al., *Inorganic nanoarchitectonics for biological applications*. Chemistry of Materials, 2011. **24**(5): p. 728-737.
8. Morris, R.E. and P.S. Wheatley, *Gas storage in nanoporous materials*. Angewandte Chemie International Edition, 2008. **47**(27): p. 4966-4981.
9. Ren, Y., Z. Ma, and P.G. Bruce, *Ordered mesoporous metal oxides: synthesis and applications*. Chemical Society Reviews, 2012. **41**(14): p. 4909-4927.
10. Ding, Y. and M. Chen, *Nanoporous metals for catalytic and optical applications*. MRS bulletin, 2009. **34**(8): p. 569-576.
11. Meek, S.T., J.A. Greathouse, and M.D. Allendorf, *Metal-organic frameworks: a rapidly growing class of versatile nanoporous materials*. Advanced Materials, 2011. **23**(2): p. 249-267.
12. Schueth, F. and W. Schmidt, *Microporous and mesoporous materials*. Advanced Materials, 2002. **14**(9): p. 629-638.
13. Simon, P. and Y. Gogotsi, *Materials for electrochemical capacitors*, in *Nanoscience and technology: a collection of reviews from Nature journals*. 2010, World Scientific. p. 320-329.

14. Ariga, K., et al., *What are the emerging concepts and challenges in NANO? Nanoarchitectonics, hand-operating nanotechnology and mechanobiology*. Polymer Journal, 2016. **48**(4): p. 371.
15. Fang, X., et al., *Hollow mesoporous aluminosilica spheres with perpendicular pore channels as catalytic nanoreactors*. ACS Nano, 2012. **6**(5): p. 4434-4444.
16. Allmaras, R., et al., *Total porosity and random roughness of the interrow zone as influenced by tillage*. 1966.
17. Ludewig, U., M. Pusch, and T.J. Jentsch, *Two physically distinct pores in the dimeric CIC-0 chloride channel*. Nature, 1996. **383**(6598): p. 340.
18. Gouda, A.M., N.K. Allam, and M.A. Swillam, *Efficient fabrication methodology of wide angle black silicon for energy harvesting applications*. RSC Advances, 2017. **7**(43): p. 26974-26982.
19. Pan, J., et al., *The closed pores of tectonically deformed coal studied by small-angle X-ray scattering and liquid nitrogen adsorption*. Microporous and Mesoporous Materials, 2016. **224**: p. 245-252.
20. Ishizaki, K., S. Komarneni, and M. Nanko, *Porous Materials: process technology and applications*. Vol. 4. 2013: Springer Science & Business Media.
21. Asadi-Eydivand, M., et al., *Effect of technical parameters on porous structure and strength of 3D printed calcium sulfate prototypes*. Robotics and Computer-Integrated Manufacturing, 2016. **37**: p. 57-67.
22. Thommes, M., et al., *Physisorption of gases, with special reference to the evaluation of surface area and pore size distribution (IUPAC Technical Report)*. Pure and Applied Chemistry, 2015. **87**(9-10): p. 1051-1069.
23. Lowell, S., et al., *Characterization of porous solids and powders: surface area, pore size and density*. Vol. 16. 2012: Springer Science & Business Media.
24. Wang, G., L. Zhang, and J. Zhang, *A review of electrode materials for electrochemical supercapacitors*. Chemical Society Reviews, 2012. **41**(2): p. 797-828.
25. Rouquerol, J., et al., *Adsorption by powders and porous solids: principles, methodology and applications*. 2013: Academic Press.

26. Yang, P., S. Gai, and J. Lin, *Functionalized mesoporous silica materials for controlled drug delivery*. Chemical Society Reviews, 2012. **41**(9): p. 3679-3698.
27. Mishra, A. and R. Prasad, *Preparation and application of perovskite catalysts for diesel soot emissions control: an overview*. Catalysis Reviews, 2014. **56**(1): p. 57-81.
28. Lu, G. and X.S. Zhao, *Nanoporous materials: science and engineering*. Vol. 4. 2004: World Scientific.
29. Polarz, S. and B. Smarsly, *Nanoporous materials*. Journal of Nanoscience and Nanotechnology, 2002. **2**(6): p. 581-612.
30. Miles, B.N., et al., *Single molecule sensing with solid-state nanopores: novel materials, methods, and applications*. Chemical Society Reviews, 2013. **42**(1): p. 15-28.
31. Parlett, C.M., K. Wilson, and A.F. Lee, *Hierarchical porous materials: catalytic applications*. Chemical Society Reviews, 2013. **42**(9): p. 3876-3893.
32. Xia, K., et al., *Hierarchical porous carbons with controlled micropores and mesopores for supercapacitor electrode materials*. Carbon, 2008. **46**(13): p. 1718-1726.
33. Crawford, G.P. and S. Zumer, *Liquid crystals in complex geometries: formed by polymer and porous networks*. 1996: CRC Press.
34. Biener, J., et al., *Nanoporous plasmonic metamaterials*. Advanced Materials, 2008. **20**(6): p. 1211-1217.
35. Pedireddy, S., et al., *One-step synthesis of zero-dimensional hollow nanoporous gold nanoparticles with enhanced methanol electrooxidation performance*. Nature Communications, 2014. **5**: p. 4947.
36. Davis, M.E., *Ordered porous materials for emerging applications*. Nature, 2002. **417**(6891): p. 813-821.
37. Seo, J.S., et al., *A homochiral metal-organic porous material for enantioselective separation and catalysis*. Nature, 2000. **404**(6781): p. 982-986.
38. Nugent, P., et al., *Porous materials with optimal adsorption thermodynamics and kinetics for CO<sub>2</sub> separation*. Nature, 2013. **495**(7439): p. 80-84.

39. Velev, O.D. and E.W. Kaler, *Structured porous materials via colloidal crystal templating: from inorganic oxides to metals*. *Advanced Materials*, 2000. **12**(7): p. 531-534.
40. Slone, R.V., et al., *Luminescent transition-metal-containing cyclophanes ('molecular squares'): covalent self-assembly, host-guest studies and preliminary nanoporous materials applications*. *Coordination chemistry reviews*, 1998. **171**: p. 221-243.
41. Barth, J.V., G. Costantini, and K. Kern, *Engineering atomic and molecular nanostructures at surfaces*, in *Nanoscience and technology: a collection of reviews from Nature journals*. 2010, World Scientific. p. 67-75.
42. Dekker, C., *Solid-state nanopores*. *Nature nanotechnology*, 2007. **2**(4): p. 209.
43. Ying, J.Y., C.P. Mehnert, and M.S. Wong, *Synthesis and applications of supramolecular-templated mesoporous materials*. *Angewandte Chemie International Edition*, 1999. **38**(1-2): p. 56-77.
44. Xing, W., et al., *Synthesis and electrochemical properties of mesoporous nickel oxide*. *Journal of Power Sources*, 2004. **134**(2): p. 324-330.
45. Scott, B.J., G. Wirnsberger, and G.D. Stucky, *Mesoporous and mesostructured materials for optical applications*. *Chemistry of Materials*, 2001. **13**(10): p. 3140-3150.
46. Vallet-Regí, M., et al., *Revisiting silica based ordered mesoporous materials: medical applications*. *Journal of Materials Chemistry*, 2006. **16**(1): p. 26-31.
47. Zhu, C., et al., *Engineering ordered and nonordered porous noble metal nanostructures: synthesis, assembly, and their applications in electrochemistry*. *Chemical Reviews*, 2015. **115**(16): p. 8896-8943.
48. Ariga, K., et al., *Nanoarchitectonics: a conceptual paradigm for design and synthesis of dimension-controlled functional nanomaterials*. *Journal of Nanoscience and Nanotechnology*, 2011. **11**(1): p. 1-13.
49. Ariga, K., et al., *Nanoarchitectonics for mesoporous materials*. *Bulletin of the Chemical Society of Japan*, 2011. **85**(1): p. 1-32.
50. Chatterjee, A., *Structure property correlations for nanoporous materials*. 2010: CRC Press.

51. Huo, Q., D.I. Margolese, and G.D. Stucky, *Surfactant control of phases in the synthesis of mesoporous silica-based materials*. Chemistry of Materials, 1996. **8**(5): p. 1147-1160.
52. Hawker, C.J. and T.P. Russell, *Block copolymer lithography: merging 'bottom-up' with 'top-down' processes*. MRS Bulletin, 2005. **30**(12): p. 952-966.
53. Pradeep, C.P., et al., *'Bottom-up' meets 'top-down' assembly in nanoscale polyoxometalate clusters: self-assembly of [P4W52O178] 24- and disassembly to [P3W39O134] 19-*. Journal of the American Chemical Society, 2008. **130**(45): p. 14946-14947.
54. Schaffer, C.B., A. Brodeur, and E. Mazur, *Laser-induced breakdown and damage in bulk transparent materials induced by tightly focused femtosecond laser pulses*. Measurement Science and Technology, 2001. **12**(11): p. 1784.
55. Mills, D., et al., *Surface texturing of Si, porous Si and TiO<sub>2</sub> by laser ablation*. Applied Surface Science, 2007. **253**(15): p. 6575-6579.
56. Hnatovsky, C., et al., *Fabrication of microchannels in glass using focused femtosecond laser radiation and selective chemical etching*. Applied Physics A: Materials Science & Processing, 2006. **84**(1): p. 47-61.
57. Mao, H. and M.A. Hillmyer, *Nanoporous polystyrene by chemical etching of poly(ethylene oxide) from ordered block copolymers*. Macromolecules, 2005. **38**(9): p. 4038-4039.
58. Magasinski, A., et al., *High-performance lithium-ion anodes using a hierarchical bottom-up approach*. Nature Materials, 2010. **9**(4): p. 353.
59. Dai, F., et al., *Bottom-up synthesis of high surface area mesoporous crystalline silicon and evaluation of its hydrogen evolution performance*. Nature Communications, 2014. **5**: p. 3605.
60. Cook, T.R., Y.-R. Zheng, and P.J. Stang, *Metal-organic frameworks and self-assembled supramolecular coordination complexes: comparing and contrasting the design, synthesis, and functionality of metal-organic materials*. Chemical Reviews, 2012. **113**(1): p. 734-777.
61. Stupp, S.I., et al., *Supramolecular materials: self-organized nanostructures*. Science, 1997. **276**(5311): p. 384-389.

62. Attard, G.S., J.C. Glyde, and C.G. Göltner, *Liquid-crystalline phases as templates for the synthesis of mesoporous silica*. *Nature*, 1995. **378**(6555): p. 366.
63. Inagaki, S., Y. Fukushima, and K. Kuroda, *Synthesis of highly ordered mesoporous materials from a layered polysilicate*. *Journal of the Chemical Society, Chemical Communications*, 1993(8): p. 680-682.
64. Langley, P. and J. Hulliger, *Nanoporous and mesoporous organic structures: new openings for materials research*. *Chemical Society Reviews*, 1999. **28**(5): p. 279-291.
65. Taylor, J., M. Brandbyge, and K. Stokbro, *Conductance switching in a molecular device: the role of side groups and intermolecular interactions*. *Physical Review B*, 2003. **68**(12): p. 121101.
66. Bruinsma, P.J., et al., *Mesoporous silica synthesized by solvent evaporation: spun fibers and spray-dried hollow spheres*. *Chemistry of Materials*, 1997. **9**(11): p. 2507-2512.
67. Sato, T., et al., *Porous biodegradable microspheres for controlled drug delivery. I. Assessment of processing conditions and solvent removal techniques*. *Pharmaceutical Research*, 1988. **5**(1): p. 21-30.
68. Chaudhari, K., et al., *Synthesis, characterization, and catalytic properties of mesoporous tin-containing analogs of MCM-41*. *Journal of Catalysis*, 1999. **183**(2): p. 281-291.
69. Das, S.K., et al., *Self-assembled mesoporous zirconia and sulfated zirconia nanoparticles synthesized by triblock copolymer as template*. *Journal of Physical Chemistry C*, 2009. **113**(20): p. 8918-8923.
70. Das, D.D. and A. Sayari, *Applications of pore-expanded mesoporous silica 6. Novel synthesis of monodispersed supported palladium nanoparticles and their catalytic activity for Suzuki reaction*. *Journal of Catalysis*, 2007. **246**(1): p. 60-65.
71. Na, K., M. Choi, and R. Ryoo, *Recent advances in the synthesis of hierarchically nanoporous zeolites*. *Microporous and Mesoporous Materials*, 2013. **166**: p. 3-19.
72. Jo, C., et al., *Multiscale phase separations for hierarchically ordered macro/mesostructured metal oxides*. *Advanced Materials*, 2017.

73. Yamauchi, Y. and K. Kuroda, *Rational design of mesoporous metals and related nanomaterials by a soft-template approach*. Chemistry—An Asian Journal, 2008. **3**(4): p. 664-676.
74. Guo, B., et al., *Soft-templated mesoporous carbon-carbon nanotube composites for high performance lithium-ion batteries*. Advanced Materials, 2011. **23**(40): p. 4661-4666.
75. Yang, P., et al., *Block copolymer templating syntheses of mesoporous metal oxides with large ordering lengths and semicrystalline framework*. Chemistry of Materials, 1999. **11**(10): p. 2813-2826.
76. Thomas, A., *Functional materials: from hard to soft porous frameworks*. Angewandte Chemie International Edition, 2010. **49**(45): p. 8328-8344.
77. Huang, L., et al., *Synthesis, morphology control, and properties of porous metal-organic coordination polymers*. Microporous and Mesoporous Materials, 2003. **58**(2): p. 105-114.
78. Holman, K.T., et al., *Metric engineering of soft molecular host frameworks*. Accounts of Chemical Research, 2001. **34**(2): p. 107-118.
79. Li, W. and D. Zhao, *An overview of the synthesis of ordered mesoporous materials*. Chemical Communications, 2013. **49**(10): p. 943-946.
80. Tang, J., et al., *Synthesis of nitrogen-doped mesoporous carbon spheres with extra-large pores through assembly of diblock copolymer micelles*. Angewandte Chemie International Edition, 2015. **54**(2): p. 588-593.
81. Petkovich, N.D. and A. Stein, *Controlling macro-and mesostructures with hierarchical porosity through combined hard and soft templating*. Chemical Society Reviews, 2013. **42**(9): p. 3721-3739.
82. Yamauchi, Y., et al., *Vapor infiltration of a reducing agent for facile synthesis of mesoporous Pt and Pt-based alloys and its application for the preparation of mesoporous Pt microrods in anodic porous membranes*. Chemistry of Materials, 2007. **20**(3): p. 1004-1011.
83. García, R., et al., *An approach toward the synthesis of platelike ordered mesoporous materials from layered zeolite precursors*. Chemistry of Materials, 2006. **18**(9): p. 2283-2292.



84. Schmidt, R., et al., *Synthesis of a mesoporous MCM-41 material with high levels of tetrahedral aluminium*. Journal of the Chemical Society, Chemical Communications, 1994. **12**: p. 1493-1494.
85. Huang, L., et al., *Investigation of synthesizing MCM-41/ZSM-5 composites*. Journal of Physical Chemistry B, 2000. **104**(13): p. 2817-2823.
86. Ciesla, U. and F. Schüth, *Ordered mesoporous materials*. Microporous and Mesoporous Materials, 1999. **27**(2-3): p. 131-149.
87. Lindén, M., et al., *Recent advances in nano-and macroscale control of hexagonal, mesoporous materials*. Journal of Porous Materials, 1998. **5**(3-4): p. 177-193.
88. Klabunde, K.J. and R.M. Richards, *Nanoscale materials in chemistry*. 2009: John Wiley.
89. Yang, P., et al., *Generalized syntheses of large-pore mesoporous metal oxides with semicrystalline frameworks*. Nature, 1998. **396**(6707): p. 152.
90. Liang, C. and S. Dai, *Synthesis of mesoporous carbon materials via enhanced hydrogen-bonding interaction*. Journal of the American Chemical Society, 2006. **128**(16): p. 5316-5317.
91. Cooper, E.R., et al., *Ionic liquids and eutectic mixtures as solvent and template in synthesis of zeolite analogues*. Nature, 2004. **430**(7003): p. 1012.
92. Cote, A.P., et al., *Porous, crystalline, covalent organic frameworks*. Science, 2005. **310**(5751): p. 1166-1170.
93. Ciesla, U., et al., *Formation of a porous zirconium oxo phosphate with a high surface area by a surfactant-assisted synthesis*. Angewandte Chemie International Edition in English, 1996. **35**(5): p. 541-543.
94. Sierra, L. and J.-L. Guth, *Synthesis of mesoporous silica with tunable pore size from sodium silicate solutions and a polyethylene oxide surfactant*. Microporous and Mesoporous Materials, 1999. **27**(2-3): p. 243-253.
95. Ma, Y., et al., *A review of zeolite-like porous materials*. Microporous and Mesoporous Materials, 2000. **37**(1-2): p. 243-252.
96. Davis, M.E., *Ordered porous materials for emerging applications*. Nature, 2002. **417**(6891): p. 813.

97. Loryuenyong, V., et al., *Synthesis of templated mesoporous silica nanoparticles under base catalysis*. Advances in Applied Ceramics, 2011. **110**(6): p. 335-339.
98. Pinnavaia, T.J. and M.F. Thorpe, *Access in nanoporous materials*. 2006: Springer Science & Business Media.
99. Schüth, F., *Non-siliceous mesostructured and mesoporous materials*. Chemistry of Materials, 2001. **13**(10): p. 3184-3195.
100. Wan, Y. and D. Zhao, *On the controllable soft-templating approach to mesoporous silicates*. Chemical Reviews, 2007. **107**(7): p. 2821-2860.
101. Bastakoti, B.P., et al., *Asymmetric block copolymers for supramolecular templating of inorganic nanospace materials*. Small, 2015. **11**(17): p. 1992-2002.
102. Li, Y., et al., *Synthesis of mesoporous TiO<sub>2</sub>/SiO<sub>2</sub> hybrid films as an efficient photocatalyst by polymeric micelle assembly*. Chemistry-A European Journal, 2014. **20**(20): p. 6027-6032.
103. Yu, C., et al., *Highly ordered mesoporous silica structures templated by poly (butylene oxide) segment di-and tri-block copolymers*. Microporous and Mesoporous Materials, 2001. **44**: p. 65-72.
104. Vivero-Escoto, J.L., et al., *Recent progress in mesoporous titania materials: adjusting morphology for innovative applications*. Science and Technology of Advanced Materials, 2012. **13**(1): p. 013003.
105. Gu, D. and F. Schüth, *Synthesis of non-siliceous mesoporous oxides*. Chemical Society Reviews, 2014. **43**(1): p. 313-344.
106. Ravikovitch, P.I., et al., *Unified approach to pore size characterization of microporous carbonaceous materials from N<sub>2</sub>, Ar, and CO<sub>2</sub> adsorption isotherms*. Langmuir, 2000. **16**(5): p. 2311-2320.
107. Sayari, A., et al., *New approaches to pore size engineering of mesoporous silicates*. Advanced Materials, 1998. **10**(16): p. 1376-1379.
108. Vallet-Regí, M., F. Balas, and D. Arcos, *Mesoporous materials for drug delivery*. Angewandte Chemie International Edition, 2007. **46**(40): p. 7548-7558.
109. Sharma, P.K., et al., *The effect of pharmaceuticals on the nanoscale structure of PEO-PPO-PEO micelles*. Colloids and Surfaces B: Biointerfaces, 2008. **61**(1): p. 53-60.

110. Zhao, D., et al., *Triblock copolymer syntheses of mesoporous silica with periodic 50 to 300 angstrom pores*. Science, 1998. **279**(5350): p. 548-552.
111. Khanal, A., et al., *Synthesis of silica hollow nanoparticles templated by polymeric micelle with core-shell-corona structure*. Journal of the American Chemical Society, 2007. **129**(6): p. 1534-1535.
112. Tanaka, S., et al., *Self-assembly of polymeric micelles made of asymmetric polystyrene-*b*-polyacrylic acid-*b*-polyethylene oxide for the synthesis of mesoporous nickel ferrite*. European Journal of Inorganic Chemistry, 2017. **2017**(10): p. 1328-1332.
113. Yu, C., B. Tian, and D. Zhao, *Recent advances in the synthesis of non-siliceous mesoporous materials*. Current Opinion in Solid State and Materials Science, 2003. **7**(3): p. 191-197.
114. Chiang, Y.D., et al., *Rational design and synthesis of cyano-bridged coordination polymers with precise control of particle size from 20 to 500 nm*. European Journal of Inorganic Chemistry, 2013. **2013**(18): p. 3141-3145.
115. Hu, M., et al., *Synthesis of superparamagnetic nanoporous iron oxide particles with hollow interiors by using prussian blue coordination polymers*. Chemistry of Materials, 2012. **24**(14): p. 2698-2707.
116. Li, X., et al., *FexCo3- xO4 nanocages derived from nanoscale metal-organic frameworks for removal of bisphenol A by activation of peroxymonosulfate*. Applied Catalysis B: Environmental, 2016. **181**: p. 788-799.
117. Ryoo, R., S.H. Joo, and S. Jun, *Synthesis of highly ordered carbon molecular sieves via template-mediated structural transformation*. Journal of Physical Chemistry B, 1999. **103**(37): p. 7743-7746.
118. Tiemann, M., *Repeated templating*. Chemistry of Materials, 2007. **20**(3): p. 961-971.
119. Velev, O.D. and A.M. Lenhoff, *Colloidal crystals as templates for porous materials*. Current Opinion in Colloid & Interface Science, 2000. **5**(1-2): p. 56-63.
120. Abeykoon, N.C., J.S. Bonso, and J.P. Ferraris, *Supercapacitor performance of carbon nanofiber electrodes derived from immiscible PAN/PMMA polymer blends*. Rsc Advances, 2015. **5**(26): p. 19865-19873.

121. Qu, Y., et al., *A simple SDS-assisted self-assembly method for the synthesis of hollow carbon nanospheres to encapsulate sulfur for advanced lithium–sulfur batteries*. Journal of Materials Chemistry A, 2013. **1**(45): p. 14306-14310.
122. Sassoze, C., et al., *Block-Copolymer-templated synthesis of electroactive RuO<sub>2</sub>-based mesoporous thin films*. Advanced Functional Materials, 2009. **19**(12): p. 1922-1929.
123. Park, J.-N., et al., *Room-temperature CO oxidation over a highly ordered mesoporous RuO<sub>2</sub> catalyst*. Reaction Kinetics, Mechanisms and Catalysis, 2011. **103**(1): p. 87-99.
124. Brezesinski, K., et al., *Ordered mesoporous  $\alpha$ -Fe<sub>2</sub>O<sub>3</sub> (hematite) thin-film electrodes for application in high rate rechargeable lithium batteries*. Small, 2011. **7**(3): p. 407-414.
125. Schiele, A., et al., *High-throughput in situ pressure analysis of lithium-ion batteries*. Analytical Chemistry, 2017. **89**(15): p. 8122-8128.
126. Brezesinski, T., et al., *Ordered mesoporous  $\alpha$ -MoO<sub>3</sub> with iso-oriented nanocrystalline walls for thin-film pseudocapacitors*. Nature Materials, 2010. **9**(2): p. 146.
127. Torad, N.L., et al., *Electric Double-layer capacitors based on highly graphitized nanoporous carbons derived from ZIF-67*. Chemistry-A European Journal, 2014. **20**(26): p. 7895-7900.
128. Dunn, B.S., et al., *Mesoporous nanocrystalline film architecture for capacitive storage devices*. 2014, Google Patents.
129. Brezesinski, T., et al., *Templated nanocrystal-based porous TiO<sub>2</sub> films for next-generation electrochemical capacitors*. Journal of the American Chemical Society, 2009. **131**(5): p. 1802-1809.
130. Tang, J., et al., *Tailored design of functional nanoporous carbon materials toward fuel cell applications*. Nano Today, 2014. **9**(3): p. 305-323.
131. Linares, N., et al., *Mesoporous materials for clean energy technologies*. Chemical Society Reviews, 2014. **43**(22): p. 7681-7717.

132. Tian, B., et al., *General synthesis of ordered crystallized metal oxide nanoarrays replicated by microwave-digested mesoporous silica*. *Advanced Materials*, 2003. **15**(16): p. 1370-1374.
133. Zhang, Z., F. Zuo, and P. Feng, *Hard template synthesis of crystalline mesoporous anatase TiO<sub>2</sub> for photocatalytic hydrogen evolution*. *Journal of Materials Chemistry*, 2010. **20**(11): p. 2206-2212.
134. Deng, J., et al., *Ultrasound-assisted nanocasting fabrication of ordered mesoporous MnO<sub>2</sub> and Co<sub>3</sub>O<sub>4</sub> with high surface areas and polycrystalline walls*. *Journal of Physical Chemistry C*, 2010. **114**(6): p. 2694-2700.
135. Li, L., et al., *Synthesis and electrochemical properties of two types of highly ordered mesoporous MnO<sub>2</sub>*. *Electrochimica acta*, 2010. **55**(5): p. 1682-1686.
136. Jiao, F., et al., *Synthesis of ordered mesoporous Fe<sub>3</sub>O<sub>4</sub> and  $\gamma$ -Fe<sub>2</sub>O<sub>3</sub> with crystalline walls using post-template reduction/oxidation*. *Journal of the American Chemical Society*, 2006. **128**(39): p. 12905-12909.
137. Tüysüz, H., et al., *Mesoporous Co<sub>3</sub>O<sub>4</sub> as an electrocatalyst for water oxidation*. *Nano Research*, 2013. **6**(1): p. 47-54.
138. Wu, Z., et al., *Ordered mesoporous crystalline  $\gamma$ -Al<sub>2</sub>O<sub>3</sub> with variable architecture and porosity from a single hard template*. *Journal of the American Chemical Society*, 2010. **132**(34): p. 12042-12050.
139. Kang, E., et al., *Ordered mesoporous WO<sub>3</sub>-X possessing electronically conductive framework comparable to carbon framework toward long-term stable cathode supports for fuel cells*. *Journal of Materials Chemistry*, 2010. **20**(35): p. 7416-7421.
140. Tian, B., et al., *General synthesis of ordered crystallized metal oxide nanoarrays replicated by microwave-digested mesoporous silica*. *Advanced Materials*, 2003. **15**(16): p. 1370-1374.
141. Wang, Y.-G. and Y.-Y. Xia, *Electrochemical capacitance characterization of NiO with ordered mesoporous structure synthesized by template SBA-15*. *Electrochimica acta*, 2006. **51**(16): p. 3223-3227.
142. Gu, D. and F. Schuth, *Synthesis of non-siliceous mesoporous oxides*. *Chemical Society Reviews*, 2014. **43**(1): p. 313-344.

143. Yang, P., et al., *Generalized syntheses of large-pore mesoporous metal oxides with semicrystalline frameworks*. Nature, 1998. **396**: p. 152.
144. Torad, N.L., et al., *Novel block copolymer templates for tuning mesopore connectivity in cage-type mesoporous silica films*. Journal of Materials Chemistry, 2012. **22**(37): p. 20008-20016.
145. Jiang, X., et al., *Synthesis of continuous mesoporous alumina films with large-sized cage-type mesopores by using diblock copolymers*. Chemistry—An Asian Journal, 2012. **7**(7): p. 1713-1718.
146. Tanaka, S., et al., *Self-assembly of polymeric micelles made of asymmetric polystyrene-*b*-polyacrylic acid-*b*-polyethylene oxide for the synthesis of mesoporous nickel ferrite*. European Journal of Inorganic Chemistry, 2017. **2017**(10): p. 1328-1332.
147. Lai, X., et al., *Ordered mesoporous NiO with thin pore walls and its enhanced sensing performance for formaldehyde*. Nanoscale, 2015. **7**(9): p. 4005-4012.
148. Tanaka, S., et al., *Mesoporous Iron oxide synthesized using poly(styrene-*b*-acrylic acid-*b*-ethylene glycol) block copolymer micelles as templates for colorimetric and electrochemical detection of glucose*. ACS Applied Materials & Interfaces, 2018. **10**(1): p. 1039-1049.
149. Kaneti, Y., et al., *Room temperature carbon monoxide oxidation over two-dimensional gold-loaded mesoporous iron oxide nanoflakes*. Chemical Communications, 2018.
150. Vijayakumar, S., S. Nagamuthu, and G. Muralidharan, *Supercapacitor studies on NiO nanoflakes synthesized through a microwave route*. ACS Applied Materials & Interfaces, 2013. **5**(6): p. 2188-2196.
151. Min, J., et al., *Self-assembly of parallelly aligned NiO hierarchical nanostructures with ultrathin nanosheet subunits for electrochemical supercapacitor applications*. ACS Applied Materials & Interfaces, 2015. **8**(1): p. 780-791.
152. Wang, X., et al., *Size-controllable porous NiO electrodes for high-performance lithium ion battery anodes*. Materials Research Bulletin, 2017. **96**: p. 533-537.
153. Bai, G., et al., *Porous NiO nanoflowers and nanourchins: highly active catalysts for toluene combustion*. Catalysis Communications, 2012. **27**: p. 148-153.

154. Yu, F., et al., *Porous NiO nano-sheet as an active and stable catalyst for CH<sub>4</sub> deep oxidation*. Applied Catalysis A: General, 2015. **507**: p. 109-118.
155. Song, X., L. Gao, and S. Mathur, *Synthesis, characterization, and gas sensing properties of porous nickel oxide nanotubes*. Journal of Physical Chemistry C, 2011. **115**(44): p. 21730-21735.
156. Ding, Y., et al., *Preparation and characterization of NiO–Ag nanofibers, NiO nanofibers, and porous Ag: towards the development of a highly sensitive and selective non-enzymatic glucose sensor*. Journal of Materials Chemistry, 2010. **20**(44): p. 9918-9926.

# Appendix 1

## Peer Reviewed Articles

1. Al-Attafi, K., Jawdat, F.H., **Qutaish, H.**, Hayes, P., Al-Keisy, A., Shim, K., Yamauchi, Y., Dou, S.X., Nattestad, A. and Kim, J.H., 2019. Cubic aggregates of  $Zn_2SnO_4$  nanoparticles and their application in dye-sensitized solar cells. Nano Energy, 57, pp.202–213.
2. **Qutaish, H.**, Tanaka, S., Kaneti, Y.V., Lin, J., Bando, Y., Alshehri, A.A., Yusa, S.I., Yamauchi, Y., Hossain, M.S.A. and Kim, J., 2018. Soft-templated synthesis of mesoporous nickel oxide using poly (styrene-block-acrylic acid-block-ethylene glycol) block copolymers. Microporous and Mesoporous Materials, 271, pp.16–22.
3. AlZoubi, T., **Qutaish, H.** and Hamzawy, S., 2018. Enhanced UV-light detection based on ZnO nanowires/graphene oxide hybrid using cost-effective low temperature hydrothermal process. Optical Materials, 77, pp.226–232.
4. Khatba, K., Paknejad, S.A., Al Zoubi, T., **Qutaish, H.**, Sano, N. and Mannan, S.H., 2018. Arresting high-temperature microstructural evolution inside sintered silver. Journal of Materials Science: Materials in Electronics, pp.1-12.

## Conference Proceedings

1. Al-Fandi, M., Oweis, R., Albiss, B.A., AlZoubi, T., Al-Akhras, M.A., **Qutaish, H.**, Khwailah, H., Al-Hattami, S. and Al-Shawwa, E., 2015. A prototype ultraviolet light sensor based on ZnO nanoparticles/graphene oxide nanocomposite using low temperature hydrothermal method. In IOP Conference Series: Materials Science and Engineering (Vol. 92, No. 1, p. 012009). IOP Publishing.